Proc Natl Acad Sci USA: doi: 10.1073/pnas.1921404117

Requirement for epithelial p38α in KRAS-driven lung tumor progression

Jessica Vitos-Faleato[1], Sebastián M. Real[1], Nuria Gutierrez-Prat[1], Alberto Villanueva[2], Elisabet Llonch[1], Matthias Drosten[3], Mariano Barbacid[3], Angel R. Nebreda[1,4,*]

[1]Institute for Research in Biomedicine (IRB Barcelona), The Barcelona Institute of Science and Technology, 08028 Barcelona, Spain
[2]Program Against Cancer Therapeutic Resistance (ProCURE), Catalan Institute of Oncology (ICO), Bellvitge Institute for Biomedical Research (IDIBELL), 08907 L'Hospitalet de Llobregat, Spain
[3]Centro Nacional de Investigaciones Oncológicas (CNIO), 28029 Madrid, Spain
[4]Institució Catalana de Recerca i Estudis Avançats (ICREA), 08010 Barcelona, Spain

* Correspondence: angel.nebreda@irbbarcelona.org, Phone +34- 934031379

JVF: orcid.org/0000-0002-9016-4695
SMR: orcid.org/0000-0001-7286-2724
NGP: orcid.org/0000-0003-1518-0158
AV: orcid.org/0000-0002-4164-6671
EL: orcid.org/0000-0003-3979-2597
MD: orcid.org/0000-0002-3205-456X
MB: orcid.org/0000-0002-1480-2624
ARN: orcid.org/0000-0002-7631-4060

Running title: p38α in lung tumor progression

Keywords: lung adenocarcinoma, KRAS, non-oncogene addiction, p38α, TIMP-1

Abstract

Malignant transformation entails important changes in the control of cell proliferation through the rewiring of selected signaling pathways. Cancer cells become then very dependent on the proper function of those pathways, and their inhibition offers therapeutic opportunities. Here we identify the stress kinase p38α as a non-oncogenic signaling molecule that enables the progression of $Kras^{G12V}$-driven lung cancer. We demonstrate *in vivo* that despite acting as a tumor suppressor in healthy alveolar progenitor cells, p38α contributes to the proliferation and malignization of lung cancer epithelial cells. We show that high expression levels of p38α correlate with poor survival in lung adenocarcinoma patients, and that genetic or chemical inhibition of p38α halts tumor growth in lung cancer mouse models. Moreover, we reveal a lung cancer epithelial cell autonomous function for p38α promoting the expression of TIMP-1, which in turn stimulates cell proliferation in an autocrine manner. Altogether, our results suggest that epithelial p38α promotes $Kras^{G12V}$-driven lung cancer progression via maintenance of cellular self-growth stimulatory signals.

Significance

Nearly half of the cases of lung cancer bear mutations in the RAS pathway. Unfortunately, no specific drugs are available to successfully target many RAS-driven tumors that are not surgically resectable. Despite the sound rationale for targeting oncogene products for cancer therapeutics, this often leads to development of resistance. As an alternative, non-oncogenic proteins can sometimes facilitate tumor progression, and even though they are neither mutated nor over-expressed in the malignant cells, they may represent potential targets for anti-cancer therapies. We have found that non-oncogenic signaling through p38α plays a tumor promoting function in lung adenocarcinoma epithelial cells by inducing the expression of TIMP-1, a growth factor-like protein. We propose that p38α inhibition could be therapeutically useful.

INTRODUCTION

Despite the many efforts invested during the past decades, the development of selective therapies remains one of the biggest challenges in oncology. Nowadays, lung adenocarcinomas in advanced stages, like those driven by mutations in EGFR or ALK, are often treated with tyrosine kinase inhibitors but, unfortunately, tumors tend to become resistant in less than a year and continue to progress (1, 2). The development of targeted therapies for KRAS-induced lung tumors has proven especially difficult. Most of the mutated KRAS forms lack suitable pockets to which drugs can bind in order to interfere with the oncogenic function, and targeting some of the downstream kinases leads to undesirable toxicities (3). An alternative approach consists on targeting synthetic lethal partners of the mutated KRAS, so that cancer cells have their viability compromised, while the normal cells without the mutated driver gene are not affected. When these partners do not have oncogenic activity themselves, the exacerbated dependency of the cancer cell for their function has been termed "non-oncogene addiction" (4). This is the case for the transcription factor GATA2 whose deletion induces the regression of established KRAS mutant lung tumors in mice (5). Therefore, charting a comprehensive map of non-oncogene addictions in KRAS-driven cancer may help to develop new therapies.

The protein kinase p38α, also known as mitogen-activated protein kinase (MAPK) 14, is normally stimulated by environmental stresses and other cues, orchestrating cell responses like proliferation, differentiation, or apoptosis depending on the stimulus and the cell type (6, 7). In the tumor context, p38α has been shown to interfere with malignant cell transformation in different tissues (8-10). In particular, p38α has been reported to suppress lung tumor formation, a function that is probably related to its ability to induce the differentiation of progenitor cells (9). Curiously, no functionally significant genomic alterations for p38α have been described in tumors, and there is evidence that p38α might be constitutively phosphorylated in several cancer types (11-13). In fact, immunohistochemistry and phospho-proteomic analysis have reported phosphorylated p38α in the tumors from non-small-cell lung carcinoma (NSCLC) patients (14-16). Both the scarcity of inactivating mutations and the presence of phosphorylated p38α in tumors suggest the possibility that cancer cells may use this non-oncogenic signaling pathway to facilitate tumor progression. Consistent with this notion, epithelial cancer cells in the intestine have been shown to exploit p38α for colon tumor maintenance *in vivo* (10). However, whether

p38α in epithelial cancer cells of other tissues contributes to tumor progression remains to be explored. Indeed, it is important to contextualize the outcomes of p38α inhibition in the different cell types of a tissue as well as the global effect of its ubiquitous downregulation given that the complex regulation of survival/death signals by p38 MAPKs can result in opposite molecular functions during tumor development, as it has been reported in UV-induced skin papillomas (17, 18) or in pancreatic ductal adenocarcinomas (19, 20). There is evidence that p38α in stromal cells can support lung tumorigenesis (21), and facilitate metastatic lung cell extravasation (22), but the contribution of p38α signaling in lung cancer epithelial cells to tumor maintenance and progression has not been investigated yet.

In this study, we have used mouse models of $Kras^{G12V}$-driven lung cancer and spheroid cultures of lung cancer cells to show a tumor-promoting role of epithelial p38α in established lung tumors.

RESULTS

p38α expression correlates with malignancy and poor prognosis in lung adenocarcinoma patients. To investigate the role of p38α in lung cancer, we first analyzed the expression levels of the *MAPK14* gene (encoding p38α) in a cohort of lung adenocarcinoma patients, formed by 107 tumor samples in stages I to IV. The levels of *MAPK14* mRNA were significantly increased in the tumors in comparison to the paired normal parenchyma (Fig. 1A). Next, in two other different cohorts of 293 and 138 samples of tumors in stages I to III with patient follow-up data, we observed that, irrespective of the tumor stage, the highest level of *MAPK14* expression correlated with a higher mortality rate (Fig. 1B), as well as with a shorter time to relapse in lung adenocarcinoma patients both in general (Fig. 1C) and in Kras-driven adenocarcinoma cohorts (See SI Appendix, fig. S1A and B). To confirm the results obtained by analyzing public mRNA datasets, we used antibodies against phosphorylated p38 or total p38α to stain a human tissue microarray, which contained samples of lung adenocarcinomas and paired adjacent normal lung tissue, as well as normal lung tissue from patients without tumors. In line with the mRNA analysis, we observed that lung tumors contained a higher number of both phosphorylated p38 and p38α-positive cells than the normal lung parenchyma (Fig. 1D and E).

In parallel, we used mice expressing $Kras^{+/FSFG12V}$, which develop lung adenocarcinomas upon intratracheal administration of adenoviruses expressing FlpO recombinase (23). Immunohistochemistry analysis confirmed a significantly increased phospho-p38 staining in $Kras^{G12V}$-driven lung tumors compared to the healthy parenchyma (Fig. 1F), supporting our observations in the lung adenocarcinoma-patient cohorts. Altogether, these results hint the implication of p38α in lung cancer, and suggest that its expression levels could be used as an independent prognostic factor for lung adenocarcinoma.

Downregulation of p38α in alveolar epithelial progenitor cells enhances $Kras^{G12V}$ lung tumorigenesis but compromises tumor progression. The correlation between *MAPK14* (p38α) expression and lung tumor malignancy was unexpected, given that p38α downregulation has been reported to sensitize lung tissue to $Kras^{G12V}$-induced oncogenic transformation (9). When mice have p38α ubiquitously downregulated, they exhibit uncontrolled proliferation of the alveolar epithelial type II (AE2) progenitor cells (8, 9), which can function as lung adenocarcinoma initiating cells (24, 25). However, since tumor-associated stromal cells can also regulate tumorigenesis, we investigated the role of p38α particularly in the alveolar progenitor cells during lung tumor development. To address this, we induced $Kras^{G12V}$ expression in lungs of mice carrying $Mapk14^{lox/lox}$ alleles and the surfactant protein C (SPC)-Cre-ER transgene, in which *Mapk14* can be specifically deleted in AE2 cells (Fig. 2A, and see SI Appendix, fig. S1C). When these mice were treated with tamoxifen, we observed a 25% downregulation of the floxed exon 2 of *Mapk14* in AE2 progenitor cells both by qRT-PCR (See SI Appendix, fig. S1D) and by using a double-fluorescent Cre reporter (See SI Appendix, fig. S1E). Consistently, 20 weeks after $Kras^{G12V}$ expression, mice with AE2 cell-specific downregulation of p38α (p38α-Δ^{SPC}) showed numerous lung tumors constituted by SPC^+ cells growing along the preexisting alveolar framework. The p38α-Δ^{SPC} tumors showed a significantly increased percentage of proliferative cells, as marked by Ki67 staining, compared to their wild-type (WT) counterparts (Fig. 2B). We also observed an increased lung weight in p38α-Δ^{SPC}; $Kras^{G12V}$ mice (See SI Appendix, fig. S1F), as well as enhanced recruitment of immune cells in their lungs (Fig. 2C), which correlated with increased STAT3 phosphorylation (See SI Appendix, fig. S1G), a well-known mediator of tumor-promoting inflammation. Accordingly, p38α-Δ^{SPC} mice showed increased lung tumor

burden (Fig. 2D). Taken together, these results support a tumor suppressor role of p38α in AE2 progenitor cells of the lung epithelia.

Surprisingly, the increased lung tumor burden observed in $Kras^{G12V}$ expressing p38α-Δ^{SPC} mice correlated with a higher percentage of early stage hyperplasias versus adenomas, compared with the tumors in $Kras^{G12V}$ expressing WT mice, in which there were more adenomas than hyperplasias (Fig. 2E). These observations suggest that p38α downregulation facilitates tumor initiation, but once the lung epithelial cells are transformed, the absence of p38α delays tumor progression to more advanced stages, hinting a possible tumor-promoting role for p38α in lung cancer cells.

p38α promotes $Kras^{G12V}$-driven lung tumor growth. If p38α is required for lung tumor progression, the acute loss of p38α in established tumors would be expected to hinder tumor growth. To test this hypothesis, we first looked at the effect of the ubiquitous downregulation of p38α using p38α-Δ^{Ub} mice, which bear *Mapk14*$^{lox/lox}$ alleles and the tamoxifen-inducible Ubiquitin C (UBC)-Cre-ERT2 transgene. The efficiency of p38α downregulation was confirmed by immunoblotting and PCR in both whole-lung lysates and individual tumors (Fig. 3A, and see SI Appendix, fig. S2A and B). Noteworthy, the levels of both total p38α and phosphorylated-p38 were higher in lungs expressing oncogenic $Kras^{G12V}$ than in healthy lung tissue (Fig. 3A). Therefore, we induced $Kras^{G12V}$ expression, confirmed the presence of lung tumors twenty weeks later and then induced p38α downregulation (Fig. 3B). Interestingly, the downregulation of p38α resulted in a significantly decreased number and size of macroscopic lung tumors in comparison to the tamoxifen-treated WT mice (*Mapk14*$^{lox/lox}$ without UBC-Cre-ERT2) (Fig. 3C). Indeed, the number and size of lung tumors in p38α-Δ^{Ub} mice were similar to those in animals analyzed at the initial time point, prior to tamoxifen injections, suggesting that p38α downregulation produced a cytostatic effect. In contrast, WT animals treated with tamoxifen showed a substantial increase in both the number of tumors and the average tumor size in comparison to the animals analyzed before p38α downregulation (Fig. 3C). This indicates that tamoxifen by itself does not interfere with lung tumor growth. As an additional control, we performed the same experiment using mice bearing UBC-Cre-ERT2 and *Mapk14*$^{+/+}$ alleles and found no significant differences upon tamoxifen treatment between WT mice and the *Mapk14*$^{+/+}$;UBC-

Cre-ERT2 control group neither in lung tumor number nor in size, ruling out any effect related to the Cre recombinase activity by itself (See SI Appendix, fig. S2C). Histological analysis of the tumors showed a remarkable decrease in the percentage of advanced lesions in p38α-Δ^{Ub} mice, with adenocarcinomas being decreased 3-fold (Fig. 3D). Collectively, these results further support the decreased ratio of advanced versus early lesions observed in p38α-Δ^{SPC} lungs, and suggest that $Kras^{G12V}$-driven lung tumors are addicted to p38α signaling.

To investigate the cause of the reduced lung tumor load observed upon p38α downregulation, we performed immunohistochemistry analysis of lung sections. We found that infiltrating lymphocytes ($CD3^+$), which remained mainly at the periphery of the tumors, and macrophages ($CD68^+$) were present in similar numbers in WT and p38α-Δ^{Ub} animals. Blood vessel distribution, as determined by $CD31^+$ staining, was also similar in tumors from both groups of mice. Likewise, we detected no differences in the number of apoptotic cells, neither by TUNEL nor by cleaved-caspase 3 staining (See SI Appendix, fig. S2D-F). However, the number of proliferating cells, as determined by Ki67 immunostaining, was significantly diminished in lung tumors from p38α-Δ^{Ub} mice (Fig. 3E). Therefore, the acute loss of p38α in developing lung tumors does not alter the numbers of infiltrating immune cells or the vasculature density, but it impairs cancer cell proliferation and tumor progression to more advanced stages.

Chemical inhibition of p38α reduces lung tumor burden in mice. The dependency of lung tumor progression on p38α is a potentially relevant observation from a clinical perspective. As a proof of principle, we used the low molecular weight chemical compound PH797804 to inhibit the kinase activity of p38α. Mice in which $Kras^{G12V}$ lung tumors had been induced 20 weeks before, were administered either PH797804 or vehicle solution via oral gavage for 14 days. We found that mice treated with the p38α inhibitor showed a significant decrease in the number and size of lung tumors in comparison to the vehicle-treated group (Fig. 4A). Inhibition of p38α signaling in the lungs was confirmed by immunoblotting analysis of Hsp27 phosphorylation, a downstream target of the pathway (Fig. 4B). Moreover, we observed that the number and size of lung tumors in mice treated with PH797804 were similar to those found before the treatment, suggesting that p38α inhibition produces a cytostatic effect. In addition, the number of advanced lesions, as well as the percentage of $Ki67^+$ cells per tumor were significantly reduced (Fig. 4C

and D). These results mirror our observations in p38α-Δ^{Ub} mice and show that the role of p38α promoting lung tumor progression is mediated through its kinase activity. Moreover, these results suggest that p38α inhibition could be potentially useful for NSCLC therapy.

Epithelial p38α is necessary for the proliferation of lung cancer cells in anchorage-independent conditions. To investigate how p38α contributes to the progression of lung tumors, we tried to induce p38α deletion in epithelial cells using mice bearing SPC-Cre-ER and $Kras^{+/FSFG12V}$ alleles but, since Cre activity was limited to roughly 25% of the AE2 cells (See SI Appendix, fig. S1D and E), the level of p38α knocked-down cells in the tumors was insufficient to draw conclusions. Therefore, to study the role of p38α in malignant lung epithelial cells, we established *ex vivo* cultures of cancer cells (named mKLC) isolated from murine $Kras^{G12V}$ lung adenocarcinomas (26). We used mice with *Mapk14*$^{lox/lox}$ alleles so that *Mapk14* can be deleted in the mKLC cells upon Cre recombinase expression, to generate p38α-deficient cells (p38α-Δ^{mKLC}). We confirmed that mKLC cells expressed the EpCAM epithelial marker and retained E-cadherin expression upon p38α downregulation (See SI Appendix, fig. S3A and B). We first looked at the proliferation capacity of the mKLC cells *in vitro*. Strikingly, we observed no differences in their cell cycle or their ability to incorporate 5-bromo-2'-deoxyuridine (BrdU) when cultured in standard monolayer conditions (See SI Appendix, fig. S3C and D). Similarly, Lewis lung carcinoma (LLC1) murine cells with p38α downregulated by shRNAs showed no differences with WT cells in BrdU incorporation (See SI Appendix, fig. S3E and F) and had no growth advantage when injected subcutaneously into the rare flanks of nude mice (See SI Appendix, fig. S3G).

Interestingly, when mKLC cells were cultured in soft agar to mimic tumor growth, we observed that WT and p38α-Δ^{mKLC} cells formed a similar number of colonies after 20 days in culture but p38α-Δ^{mKLC} colonies were significantly smaller (Fig. 5A). In a complementary experiment, we noticed that inducing the downregulation of p38α in established colonies formed by mKLC cells slowed down their growth (See SI Appendix, fig. S3H). These results were confirmed using H358 human lung cancer cells, which also formed smaller colonies in soft agar in the presence of two different p38α chemical inhibitors (See SI Appendix, fig. S3I).

Consistent with the above observations, both WT and p38α-Δ^{mKLC} cells intratracheally implanted in immunocompetent mice formed a similar number of lung tumors (Fig. 5B). However, tumors formed by p38α-Δ^{mKLC} cells showed a significantly decreased size and less proliferative cells (Fig. 5C and D). Likewise, we implanted mKLC cells expressing Cre-ERT2 intratracheally into C57BL/6 mice and, once lung tumors were formed, p38α downregulation was induced *in vivo*. We found that p38α downregulation significantly diminished the number and size of the lung tumors (Fig. 5E), phenocopying the results observed using the UBC-Cre-ERT2;$Kras^{+/FSFG12V}$ mice. Importantly, these data indicate that the proliferation assays in 2D cell cultures and subcutaneous xenografts do not reproduce the *in vivo* scenario in lung tumors upon p38α downregulation. Instead, p38α signaling appears to have an important contribution to the proliferation of $Kras^{G12V}$-driven epithelial lung cancer cells when these cells are challenged by culturing in anchorage-independent conditions or by orthotopic implantation in mice.

To further understand the role of p38α in lung tumor progression, we investigated the effect of p38α depletion on the metastatic features of mKLC cells. We found that both WT and p38α-deficient cells showed equivalent adhesion and migration capacities, resistance to anoikis, and extravasation abilities (See SI Appendix, fig. S4A-D). We next confirmed these results by implanting WT and p38α-Δ^{mKLC} cells into the rare flanks of immunodeficient mice. The number of lung metastatic foci detected two weeks after primary tumor resection was similar in both groups, indicating a similar ability of p38α-Δ^{mKLC} and WT cells to disseminate and colonize the lung (See SI Appendix, fig. S4E). However, when we injected LLC1 cells through the tail vein of nude mice, we observed two weeks later a smaller lung tumor burden in animals injected with p38α-deficient cells (See SI Appendix, fig. S4F). The difference in lung tumor area but not in metastatic dissemination ability suggests that p38α does not impact on the metastatic properties of the epithelial lung cancer cells, but mainly affects their proliferation rate and hence the tumor mass growth rate.

p38α-mediated expression of TIMP-1 induces lung cancer cell proliferation. There is evidence that p38α can regulate both the expression of cytokines and the transducing signaling pathways engaged by these factors, which can stimulate cancer cell proliferation (11). Therefore, we analyzed the possibility that secreted factors controlled by p38α could self-stimulate the

proliferation of lung cancer cells. We used an antibody array to check the expression of 40 cytokines in lung tumors formed by the orthotopic inoculation of either WT or p38α-Δ^{mKLC} cells, and validated the results in individual tumors by qRT-PCR (See SI Appendix, fig. S5A-C). We identified TIMP-1 as one of the most significantly downregulated cytokines (Fig. 6A). Moreover, p38α downregulation in lung tumors resulted in decreased levels of *Timp1* mRNA (Fig. 6B). Accordingly, TIMP-1 protein levels in p38α-deficient mouse lungs, either healthy or bearing $Kras^{G12V}$-driven tumors, were decreased in comparison to the equivalent WT lungs (Fig. 6C).

TIMP-1 is an inhibitor of matrix metalloproteinases that can also promote lung tumor growth through its binding to CD63 (27), and is usually expressed at high levels in lung cancer patients with poor prognosis (28, 29). Hence, we investigated whether the reduced *Timp1* expression was responsible for the impaired proliferation of p38α-deficient lung cancer cells. First, we analyzed *Timp1* mRNA levels in epithelial cancer cells sorted from mouse lung tumors, and observed that *Timp1* expression was dependent on p38α (See SI Appendix, fig. S5D). We also obtained evidence of TIMP-1 implication in epithelial lung cancer cell proliferation by using two different TIMP-1 shRNAs, which reduced the size of colonies formed by mKLC cells grown in soft agar, an effect that was attenuated in the presence of recombinant TIMP-1 (Fig. 6D and E). Moreover, the addition of recombinant TIMP-1 also rescued the decreased colony size observed in p38α-deficient mKLC cells grown in soft agar (Fig. 6F). Similar results were observed adding recombinant TIMP-1 to human H460 and murine mKLC cells treated with p38α chemical inhibitors (Fig. 6G, and see SI Appendix, fig. S5E). Interestingly, analysis of public gene expression databases revealed a direct correlation between the expression of *Timp1* and *MAPK14* mRNAs in human adenocarcinomas (See SI Appendix, fig. S5F). Therefore, the proliferation of lung cancer epithelial cells is regulated by the levels of TIMP-1 which, in turn, are controlled by p38α.

In fact, the p38α regulated transcription factors AP-1 and ATF-2 have binding sites on the *Timp1* promoter, which also contains two NFκB binding sites (30), and the NFκB pathway has been shown to control TIMP-1 levels in a mouse lung cancer model (27). Since TIMP-1 expression controls lung cancer cell proliferation (Fig. 6E), we hypothesized that inhibition of NFκB signaling would phenocopy p38α inhibition. Treatment of soft agar colonies formed by

mKLC cells with an inhibitor of IKK2, a kinase upstream of p65 NFκB, resulted in decreased colony size, which was further decreased by the combined treatment with both p38α and IKK2 inhibitors (See SI Appendix, fig. S5G). Altogether, these results support a key role for TIMP-1 in Kras-driven lung cancer, indicating that TIMP-1 promotes epithelial lung cancer cell proliferation in an autocrine manner, and that both p38α and NFκB signaling contribute to TIMP-1 production by epithelial cancer cells.

DISCUSSION

Given the plethora of cellular processes that p38α can regulate, its role in tumorigenesis has been hard to define. Depending on the nature of the stimulus, the cell type and the malignant stage, p38α is involved in cell death or survival, cell cycle entry or induction of cell differentiation, (11, 31). Therefore, it is difficult to predict which tumors could benefit from p38α inhibition without performing *in vivo* experiments.

Here, we use mouse models of KRAS-driven NSCLC to show that p38α plays a dual role during lung tumorigenesis. We provide evidence that p38α plays a tumor suppressor function in normal lung epithelial cells, interfering with $Kras^{G12V}$-driven malignant transformation. In this case, p38α maintains the homeostasis by balancing proliferation and differentiation capacities of alveolar progenitors (9), and maybe also by mediating senescence entry induced by oncogenic Kras expression, as shown in cultured fibroblasts (32) (33). Therefore, in the absence of p38α there is an increased number of poorly differentiated epithelial cells with the potential to become tumor initiating cells (9). In addition to the deregulated proliferation of the progenitor cells, p38α-deficient lungs have an enhanced immune response, as indicated by the increased number of $CD45^+$ cells recruited. These immune cells probably belong to the myeloid lineage (8), and collaterally contribute to tumor-promoting inflammation. Despite the benefits that the downregulation of p38α would entail *a priori* for tumor development, lung cancer cells do not seem to shut off this anticancer signaling pathway. Instead, we detect increased phosphorylated p38α in lung tumors compared to paired healthy parenchyma, which agrees with previous reports on NSCLC patients (14-16). Moreover, we show that higher p38α levels correlate with poor overall survival and with recurrence in lung adenocarcinoma, as it was proposed for colorectal cancer (34). Our results indicate that during tumor progression, lung cancer cells get advantage

of the ability of p38α to regulate targets like TIMP-1, a metalloproteinase inhibitor that not only regulates extracellular matrix catabolism but also promotes cell proliferation and survival in an autocrine manner. This latter function of TIMP-1 is based on both the regulation of the pericellular availability of protease-dependent growth factor or cytokine signals, and the binding to CD44/pro-MMP9 or to CD63, which in turn can stimulate ERK, FAK, YAP/TAZ and PI3K signaling pathways (35, 36). Accordingly, clinical studies have positively correlated high Timp-1 expression levels with poor prognosis in lung and colon cancer patients, as well as with short relapse-time and advanced-stage tumors from breast and brain origin (37).

It has been reported that the IKK2/NFκB and p38 MAPK/ATF-2 pathways can both induce *Timp1* transcription in IL-1-stimulated human astrocytes, consistent with the presence of AP-1, NFκB and ATF-2 binding sites on the *Timp1* promoter (30). A previous study also showed that IKK2 downregulation decreases tumor cell proliferation in a mouse model of lung cancer, which correlates with decreased expression of TIMP-1 (27), mirroring the phenotype of p38α downregulation. Here we show that chemical inhibition of either p38α or IKK2 impairs the proliferation of epithelial lung cancer cells in soft agar. Of note, p38α and NFκB can coordinately control the expression of several genes, such as the CXCL10 cytokine (38, 39), which we also found downregulated in p38α-deficient lung tumors. In fact, p38α has been reported to target IκBα for degradation (40), and to modulate the acetylation of p65, hence controlling the transcriptional activity of NFκB (41). Therefore, it seems likely that both pathways might perform overlapping functions in lung tumor progression. It would be interesting to test whether the combined inhibition of p38α and IKK2 could prevent any compensatory cross-talk and suffice to trigger lung tumor regression instead of the cytostatic effect observed upon inhibition of either single pathway alone.

Our studies identify p38α as a synthetic lethal interactor of $Kras^{G12V}$ in lung epithelial cancer cells, suggesting its potential interest as a therapeutic target. As prove of concept, we used the p38α pharmacological inhibitor PH-797804 that reached phase II clinical trials for chronic obstructive pulmonary disease (42). Treatment with PH797804 showed that p38α activity is required for the progression of genetically-induced lung tumors to advanced stages. In addition, orthotopic xenograft experiments indicated that epithelial cancer cells rely on p38α signaling to proliferate within the pulmonary niche *in vivo*. Although metastatic properties of lung cancer

cells do not seem to depend on p38α, our results indicate that the malignancy and size of the lung tumor mass is ultimately determined by the epithelial p38α levels. This dependency on p38α is highlighted by the anchorage-independent proliferation assays using lung epithelial cancer cells *ex vivo*, and agrees with a report for signet-ring carcinoma cell lines that also form smaller colonies when treated with the p38 MAPK inhibitor SB203580 (43). Taken together, our data indicate a pro-tumorigenic function of p38α in epithelial cancer cells of KRAS-driven lung tumors.

There is evidence that p38α can also mediate non-cancer cell autonomous functions in lung tumors. Ubiquitous expression of a non-phosphorylatable p38α mutant has been reported to impair the synthesis of hyaluronic acid by cancer-associated fibroblasts, reducing lung cancer cell proliferation (21). p38α can also regulate PD-L1 expression in $Kras^{G12V}$-driven cancer cells, thus impairing the tumor immunosurveillance capacity (44). Moreover, p38α might control the ability of infiltrating myeloid cells to contribute to lung adenocarcinoma progression, as described in colon cancer via IGF-1 production (45). Therefore, p38α seems to control the production of different extracellular factors that will build autocrine and reciprocal signaling circuitries between stromal and cancer cells, in a way comparable to the circuitry established by human lung stem cells and their niche (46). These results support the use of pharmacological inhibitors of p38α to target pro-tumorigenic functions of both cancer cells and stromal cells in lung tumors.

Whether the dependency on p38α for lung tumor progression is restricted to KRAS mutant tumors or it applies to other lung tumors independently of the driver mutation remains to be investigated. In the case of lung tumors with non-functional p53, which account for about half of NSCLC cases (47), it has been reported that mice systemically expressing non-phosphorylatable p38α show decreased $Kras^{G12D}$-induced tumor burden (21). Moreover, our results using the human cancer cell lines H460 ($p53^{wt}$) and H358 (p53-deleted) suggest that epithelial p38α facilitates soft-agar growth independently of the p53 status. It should be also noted that p38α has been reported to facilitate resistance of lung tumors to cisplatin *in vivo* in both p53-proficient and -deficient mouse models (48, 49). Therefore, the requirement for p38α signaling in cancer cell fitness and in its interaction with the stroma is likely to represent a selective difference between normal cells and cancer cells in different tumor types, which can be

exploited to treat lung adenocarcinoma and perhaps to improve the efficacy of currently used drugs.

METHODS

Mice. Kras$^{+/FSFG12V}$ mice (23) were crossed with *Mapk14*$^{lox/lox}$ (9, 50), *Mapk14*$^{+/-}$ (51) and UBC-Cre-ERT2 mice (52) to obtain the genotypes *Mapk14*$^{lox/lox}$;Ub-CreERT2;Kras$^{+/FSFG12V}$ and *Mapk14*$^{lox/-}$;Ub-CreERT2;Kras$^{+/FSFG12V}$, which both gave indistinguishable phenotypes. Kras$^{+/FSFG12V}$*Mapk14*$^{lox/lox}$ were alternatively crossed to Sftpc-Cre-ER mice (53) to obtain mice with lung-specific p38α downregulation (p38α-Δ^{SPC}). The two p38α deficient mouse lines were on a mixed C57BL/6-FVB background and showed indistinguishable lung phenotypes, as determined by histology studies. Littermate controls of both sexes were used in all experiments. Mice were housed according to the national and European Union regulations, and protocols were approved by the animal care and use committee of both the Barcelona Science Park (PCB) and Biomedical Research Park of Barcelona (PRBB).

Generation of mKLC cells and p38α downregulation *ex vivo*. Primary adenocarcinomas generated in *Mapk14*$^{lox/lox}$;Kras$^{+/FSFG12V}$ mice were orthotopically implanted in Crl:NU-Foxn1nu mice as previously described (26). A freshly collected fragment of lung tumor was minced with sterile scalpels and then was plated in Dulbecco's modified Eagle medium (DMEM) supplemented with 20% fetal bovine serum (FBS) plus 1% penicillin/streptomycin. Medium was renewed once a week until colonies with epithelial cell morphology were observed. Then cells were trypsinized and expanded as established cell lines.

To downregulate p38α, mKLC cells with *Mapk14*$^{lox/lox}$ alleles were treated with Tat-Cre recombinant protein (54) at a concentration of 150 μg/ml in serum-free DMEM with 1% penicillin/streptomycin. After 10 h, medium was replaced with DMEM 10% FBS, and cells were passaged twice before performing experiments. For mKLC cells carrying both *Mapk14*$^{lox/lox}$ alleles and inducible Cre-ERT2, p38α downregulation was induced by treating with 4OHT-TMX (10 μM, Sigma #H6278) for 3 days.

Orthotopic implantation. Immunocompetent mice were anesthetized, intratracheally inoculated with 100 μl of a 2x10^6 mKLC cells/ml solution, and tumors were left to grow for 25 days. For

intratracheal administration, cells were cultured to 70% confluence in DMEM 10% FBS, diluted with PBS, kept on ice, and thoroughly mixed prior to each inoculation. The vocal cords were viewed directly with the help of a cold light source, and a blunted catheter coupled to a syringe was passed beyond them to inoculate the cells.

Histopathological analysis and immunohistochemistry. Mouse lungs were fixed by insufflating 10% neutral buffered formalin (Sigma) through the trachea with a syringe, incubated overnight at 4°C in 10 ml 10% neutral buffered formalin, and then embedded in paraffin. Tumors in freshly harvested lungs were counted and sized, and lung sections stained with hematoxylin and eosin (H&E) were analyzed for tumor grade by two independent observers in a blinded fashion. Tumor grade was evaluated following established classifications (55). The human lung cancer tissue array (US Biomax Inc., HLug-Ade050CD-01) included lung adenocarcinoma samples with adjacent normal tissues, and samples of normal lung from patients without tumor. After staining, it was evaluated blindly by three independent observers. Slides were incubated using the following antibodies: CD31 (Abcam # 28364; 1:500), CD45 (BD biosciences #550539; 1:100), CD68 (Biorbyt #47985; 1:750), Cleaved Caspase-3 (Cell Signaling #9661; 1:500), Ki67 (Novacastra, #NCL-Ki67p; 1:500), p38α (Cell Signaling #9218; 1:50), phospho-Thr180/Tyr182 p38 MAPK (Cell Signaling #4631; 1:50), phospho-Thr334 MK2 (Cell Signaling #3007; 1:100), phospho-Tyr705 STAT3 (Cell Signaling #9145S; 1:200), pro-SPC (Millipore #AB3786; 1:3000), and HRP conjugated secondaries (ImmunoLogic and Dako). Immunostaining was visualized with 3, 3-diaminobenzidine, and counterstained with hematoxylin, or subsequently incubated with Alexa-conjugated secondary antibodies (Life Technologies #A21441; 1:400). To detect apoptosis in paraffin-embedded samples, the Fluorescein in situ cell death detection kit (Roche #11684795910) was used according to manufacturer's instructions.

Whole digital slides were acquired with a slide scanner (Nanozoomer, Hamamatsu), and individual images were captured with NDP view software. All tumors in each tissue section were analyzed. Positive signals were quantified in an automated manner based on either the relative percentage of stained surface in a tumor or the relative percentage of positive cells per tumor, using computerized imaging software (Image J).

Statistical methods. Data are presented as means ± standard error of the mean (SEM), unless otherwise indicated. Dataset statistics were analyzed with Prism 7 (GraphPad software). Groups were compared using the two tailed Mann-Whitney test or the analysis of variance (ANOVA, Kruskal-Wallis). p values smaller than 0.05 were considered statistically significant: *, $p<0.05$, **, $p<0.01$, ***p, <0.001, ****, $p<0.0001$.

Data availability statement. All data discussed in the paper will be made available to readers.

ACKNOWLEDGEMENTS

We thank M. Onaitis for kindly providing the SPC-Cre mouse, E. Brown for UBC-Cre-ERT2 mice, M. Pasparakis for the plasmid to express Tat-Cre protein, and A. Igea for the purified Tat-Cre protein. We acknowledge the technical assistance of August Vidal from Hospital Universitari de Bellvitge, Neus Prats and the IRB Histology facility members, Camille Stephan-Otto Attolini and Oscar Reina from the IRB Biostatistics/Bioinformatics facility, the IRB Genomics Unit, and Jaume Comas and the UB Fluorescence-Activated Cell Sorting facility members. We are grateful to Sara Mainardi and Carmen Guerra for insights into lung tumor histopathology, Jordi Hernández, Raquel Batlle, Antonio Maraver, David Santamaria, Chiara Ambrogio and Monica Cubillos-Rojas for helpful suggestions and support, and Ivan del Barco for input early in the project. This work was supported by grants from the European Research Council (ERC 294665), the Ministerio de Ciencia, Innovación y Universidades (MICINN) (BFU2010-17850 and SAF2016-81043-R), Agència de Gestió D'Ajuts Universitaris I de Recerca (AGAUR) (2017 SRG-557) and the Fundación Banco Bilbao Vizcaya Argentaria (BBVA). J.V.F. acknowledges a Formación de Personal Investigador (FPI) predoctoral fellowship. IRB Barcelona is the recipient of institutional funding from MICINN through the Centres of Excellence Severo Ochoa award and from the Centres de Recerca de Catalunya (CERCA) Program of the Catalan Government.

AUTHOR CONTRIBUTIONS

J.V.-F. designed and performed the experiments, analyzed data and wrote the manuscript, S.M.R. designed and performed experiments with LLC1 cells and analyzed data; N.G-P performed experiments with TIMP-1 downregulated cell lines, A.V. generated cell lines from

mouse lung tumors, E.L. processed histology samples, M.D. and M.B. provided the $Kras^{G12V}$-expressing mouse, protocols, reagents and essential advice to use them. A.R.N. provided funding, supervised the overall study, designed experiments, analyzed data, and wrote the manuscript.

The authors declare no conflict of interest

REFERENCES

1. W. D. Travis *et al*., The 2015 World Health Organization Classification of Lung Tumors: Impact of Genetic, Clinical and Radiologic Advances Since the 2004 Classification. *J Thorac Oncol* **10**, 1243-1260 (2015).
2. L. Bombardelli, A. Berns, The steady progress of targeted therapies, promising advances for lung cancer. *Ecancermedicalscience* **10**, 638 (2016).
3. R. B. Blasco *et al*., c-Raf, but not B-Raf, is essential for development of K-Ras oncogene-driven non-small cell lung carcinoma. *Cancer Cell* **19**, 652-663 (2011).
4. R. Nagel, E. A. Semenova, A. Berns, Drugging the addict: non-oncogene addiction as a target for cancer therapy. *EMBO Rep* **17**, 1516-1531 (2016).
5. M. S. Kumar *et al*., The GATA2 transcriptional network is requisite for RAS oncogene-driven non-small cell lung cancer. *Cell* **149**, 642-655 (2012).
6. A. Cuenda, S. Rousseau, p38 MAP-kinases pathway regulation, function and role in human diseases. *Biochim Biophys Acta* **1773**, 1358-1375 (2007).
7. A. Cuadrado, A. R. Nebreda, Mechanisms and functions of p38 MAPK signalling. *Biochem J* **429**, 403-417 (2010).
8. L. Hui *et al*., p38alpha suppresses normal and cancer cell proliferation by antagonizing the JNK-c-Jun pathway. *Nat Genet* **39**, 741-749 (2007).
9. J. J. Ventura *et al*., p38alpha MAP kinase is essential in lung stem and progenitor cell proliferation and differentiation. *Nat Genet* **39**, 750-758 (2007).
10. J. Gupta *et al*., Dual function of p38alpha MAPK in colon cancer: suppression of colitis-associated tumor initiation but requirement for cancer cell survival. *Cancer Cell* **25**, 484-500 (2014).
11. E. F. Wagner, A. R. Nebreda, Signal integration by JNK and p38 MAPK pathways in cancer development. *Nat Rev Cancer* **9**, 537-549 (2009).
12. A. P. Leelahavanichkul K, Molinolo AA, Basile JR, Koontongkaew S, Gutkind JS, A role for p38 MAPK in head and neck cancer cell growth and tumor-induced angiogenesis and lymphangiogenesis. *Mol Oncol* **8**, 105-118 (2014).
13. B. Gil-Araujo *et al*., Dual specificity phosphatase 1 expression inversely correlates with NF-kappaB activity and expression in prostate cancer and promotes apoptosis through a p38 MAPK dependent mechanism. *Mol Oncol* **8**, 27-38 (2014).
14. A. K. Greenberg *et al*., Selective p38 activation in human non-small cell lung cancer. *Am J Respir Cell Mol Biol* **26**, 558-564 (2002).

15. G. Mountzios *et al*., Mitogen-activated protein kinase activation in lung adenocarcinoma: a comparative study between ever smokers and never smokers. *Clin Cancer Res* **14**, 4096-4102 (2008).
16. K. Rikova *et al*., Global survey of phosphotyrosine signaling identifies oncogenic kinases in lung cancer. *Cell* **131**, 1190-1203 (2007).
17. K. Liu *et al*., Sunlight UV-induced skin cancer relies upon activation of the p38alpha signaling pathway. *Cancer research* **73**, 2181-2188 (2013).
18. H. Zheng *et al*., A posttranslational modification cascade involving p38, Tip60, and PRAK mediates oncogene-induced senescence. *Mol Cell* **50**, 699-710 (2013).
19. M. Korc, p38 MAPK in pancreatic cancer: finding a protective needle in the haystack. *Clin Cancer Res* **20**, 5866-5868 (2014).
20. M. S. Alam *et al*., Selective inhibition of the p38 alternative activation pathway in infiltrating T cells inhibits pancreatic cancer progression. *Nat Med* **21**, 1337-1343 (2015).
21. A. Brichkina *et al*., p38MAPK builds a hyaluronan cancer niche to drive lung tumorigenesis. *Genes Dev* **30**, 2623-2636 (2016).
22. Y. Matsuo *et al*., Involvement of p38alpha mitogen-activated protein kinase in lung metastasis of tumor cells. *J Biol Chem* **281**, 36767-36775 (2006).
23. M. Sanclemente *et al*., c-RAF Ablation Induces Regression of Advanced Kras/Trp53 Mutant Lung Adenocarcinomas by a Mechanism Independent of MAPK Signaling. *Cancer Cell* **33**, 217-228 e214 (2018).
24. S. Mainardi *et al*., Identification of cancer initiating cells in K-Ras driven lung adenocarcinoma. *Proc Natl Acad Sci USA* **111**, 255-260 (2014).
25. K. D. Sutherland *et al*., Multiple cells-of-origin of mutant K-Ras-induced mouse lung adenocarcinoma. *Proc Natl Acad Sci USA* **111**, 4952-4957 (2014).
26. C. Ambrogio *et al*., Modeling lung cancer evolution and preclinical response by orthotopic mouse allografts. *Cancer research* **74**, 5978-5988 (2014).
27. Y. Xia *et al*., Reduced cell proliferation by IKK2 depletion in a mouse lung-cancer model. *Nat Cell Biol* **14**, 257-265 (2012).
28. I. S. Aljada *et al*., Upregulation of the tissue inhibitor of metalloproteinase-1 protein is associated with progression of human non-small-cell lung cancer. *J Clin Oncol* **22**, 3218-3229 (2004).
29. M. Pesta *et al*., Prognostic significance of TIMP-1 in non-small cell lung cancer. *Anticancer Res* **31**, 4031-4038 (2011).
30. K. M. Wilczynska *et al*., A novel mechanism of tissue inhibitor of metalloproteinases-1 activation by interleukin-1 in primary human astrocytes. *J Biol Chem* **281**, 34955-34964 (2006).
31. A. Igea, A. R. Nebreda, The Stress Kinase p38alpha as a Target for Cancer Therapy. *Cancer research* **75**, 3997-4002 (2015).
32. W. Wang *et al*., Sequential activation of the MEK-extracellular signal-regulated kinase and MKK3/6-p38 mitogen-activated protein kinase pathways mediates oncogenic ras-induced premature senescence. *Mol Cell Biol* **22**, 3389-3403 (2002).
33. A. Freund, C. K. Patil, J. Campisi, p38MAPK is a novel DNA damage response-independent regulator of the senescence-associated secretory phenotype. *EMBO J* **30**, 1536-1548 (2011).
34. X. J. Fan *et al*., Phosphorylated p38, a negative prognostic biomarker, complements TNM staging prognostication in colorectal cancer. *Tumour Biol* **35**, 10487-10495 (2014).

35. B. Grunwald, B. Schoeps, A. Kruger, Recognizing the Molecular Multifunctionality and Interactome of TIMP-1. *Trends Cell Biol* **29**, 6-19 (2019).
36. T. Ando *et al*., Tissue inhibitor of metalloproteinase-1 promotes cell proliferation through YAP/TAZ activation in cancer. *Oncogene* **37**, 263-270 (2018).
37. H. W. Jackson, V. Defamie, P. Waterhouse, R. Khokha, TIMPs: versatile extracellular regulators in cancer. *Nat Rev Cancer* **17**, 38-53 (2017).
38. S. Saccani, S. Pantano, G. Natoli, p38-Dependent marking of inflammatory genes for increased NF-kappa B recruitment. *Nat Immunol* **3**, 69-75 (2002).
39. C. K. Wong, C. B. Wang, W. K. Ip, Y. P. Tian, C. W. Lam, Role of p38 MAPK and NF-kB for chemokine release in coculture of human eosinophils and bronchial epithelial cells. *Clin Exp Immunol* **139**, 90-100 (2005).
40. P. Viatour, M. P. Merville, V. Bours, A. Chariot, Phosphorylation of NF-kappaB and IkappaB proteins: implications in cancer and inflammation. *Trends Biochem Sci* **30**, 43-52 (2005).
41. R. N. Saha, M. Jana, K. Pahan, MAPK p38 regulates transcriptional activity of NF-kappaB in primary human astrocytes via acetylation of p65. *J Immunol* **179**, 7101-7109 (2007).
42. W. MacNee, R. J. Allan, I. Jones, M. C. De Salvo, L. F. Tan, Efficacy and safety of the oral p38 inhibitor PH-797804 in chronic obstructive pulmonary disease: a randomised clinical trial. *Thorax* **68**, 738-745 (2013).
43. Q. Xu *et al*., The PI 3-kinase-Rac-p38 MAP kinase pathway is involved in the formation of signet-ring cell carcinoma. *Oncogene* **22**, 5537-5544 (2003).
44. M. A. Coelho *et al*., Oncogenic RAS Signaling Promotes Tumor Immunoresistance by Stabilizing PD-L1 mRNA. *Immunity* **47**, 1083-1099 e1086 (2017).
45. C. Youssif *et al*., Myeloid p38alpha signaling promotes intestinal IGF-1 production and inflammation-associated tumorigenesis. *EMBO Mol Med* **10**, pii: e8403 (2018).
46. E. J. Ruiz, F. Oeztuerk-Winder, J. J. Ventura, A paracrine network regulates the cross-talk between human lung stem cells and the stroma. *Nat Commun* **5**, 3175 (2014).
47. Z. Chen, C. M. Fillmore, P. S. Hammerman, C. F. Kim, K. K. Wong, Non-small-cell lung cancers: a heterogeneous set of diseases. *Nat Rev Cancer* **14**, 535-546 (2014).
48. S. Morandell *et al*., A reversible gene-targeting strategy identifies synthetic lethal interactions between MK2 and p53 in the DNA damage response in vivo. *Cell Rep* **5**, 868-877 (2013).
49. A. Brichkina *et al*., Proline isomerisation as a novel regulatory mechanism for p38MAPK activation and functions. *Cell Death Differ* **23**, 1592-1601 (2016).
50. J. Heinrichsdorff, T. Luedde, E. Perdiguero, A. R. Nebreda, M. Pasparakis, p38 alpha MAPK inhibits JNK activation and collaborates with IkappaB kinase 2 to prevent endotoxin-induced liver failure. *EMBO Rep* **9**, 1048-1054 (2008).
51. R. H. Adams *et al*., Essential role of p38alpha MAP kinase in placental but not embryonic cardiovascular development. *Mol. Cell* **6**, 109-116. (2000).
52. Y. Ruzankina *et al*., Deletion of the developmentally essential gene ATR in adult mice leads to age-related phenotypes and stem cell loss. *Cell Stem Cell* **1**, 113-126 (2007).
53. X. Xu *et al*., Evidence for type II cells as cells of origin of K-Ras-induced distal lung adenocarcinoma. *Proc Natl Acad Sci USA* **109**, 4910-4915 (2012).
54. M. Peitz, K. Pfannkuche, K. Rajewsky, F. Edenhofer, Ability of the hydrophobic FGF and basic TAT peptides to promote cellular uptake of recombinant Cre recombinase: a tool for

efficient genetic engineering of mammalian genomes. *Proc Natl Acad Sci USA* **99**, 4489-4494 (2002).
55. E. L. Jackson *et al*., Analysis of lung tumor initiation and progression using conditional expression of oncogenic K-ras. *Genes Dev* **15**, 3243–3248 (2001).

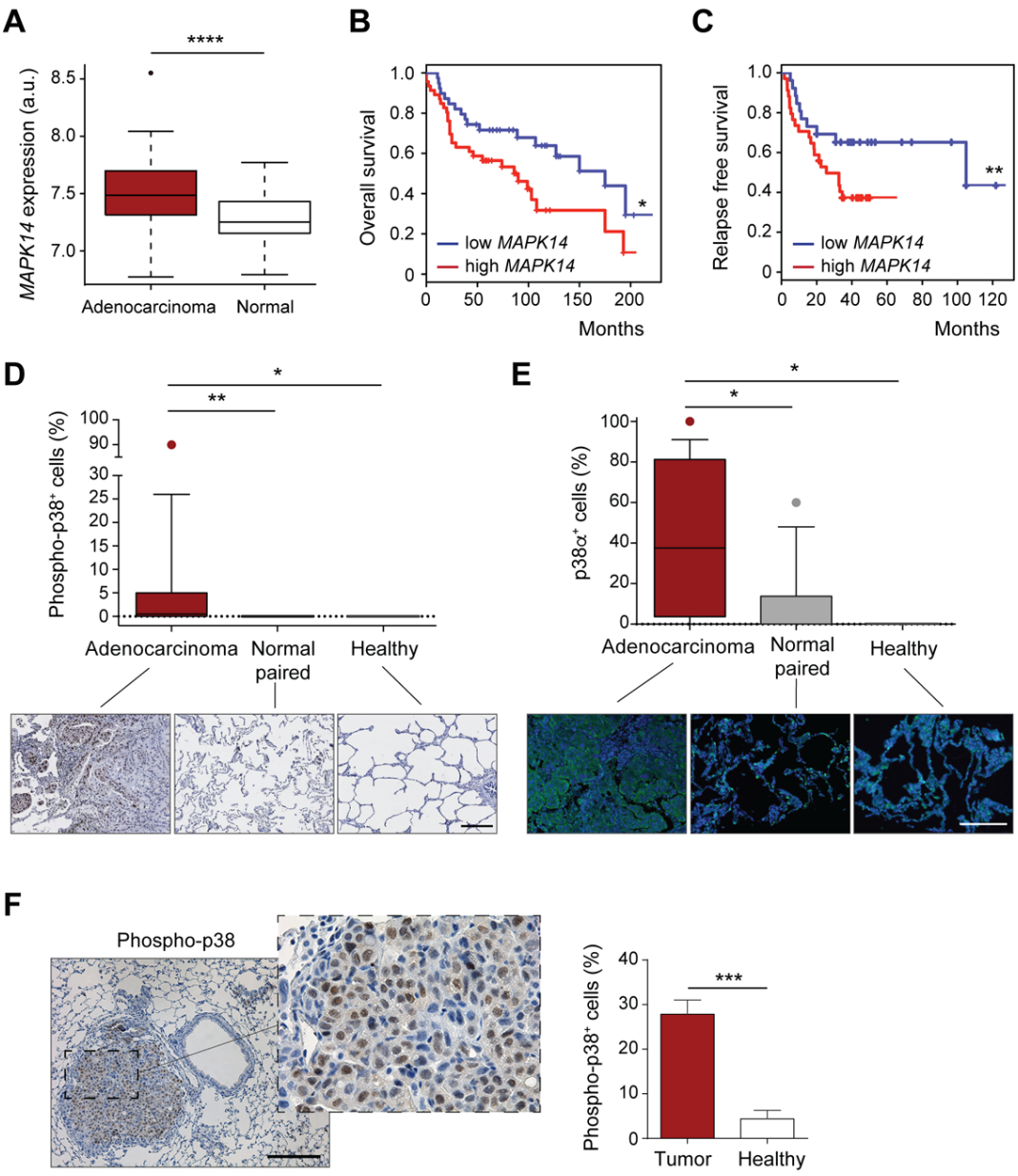

Fig. 1. High levels of p38α expression correlate with malignancy and poor prognosis. (A) Boxplots for expression levels of *MAPK14* mRNA comparing paired adenocarcinomas and healthy tissues (n≥49 per group). a.u., arbitrary units. (B) Kaplan–Meier plots showing a univariate analysis of overall survival of lung adenocarcinoma patients stratified by high or low *MAPK14* mRNA expression (n≥39 per group). (C) Kaplan-Meier plots displaying a recurrence-free survival over time of lung adenocarcinoma patients stratified by high or low *MAPK14* mRNA expression (n≥26 per group). (D) Representative images and boxplot of the percentage of

phospho-p38^{+} cells in lung adenocarcinoma tumors (n=17), paired normal tissue (n=14) and healthy lung parenchyma (n=5) from a human tissue array. Scale bar, 200 μm. (E) Same samples as in (D) were stained with a p38α antibody by immunofluorescence. Dapi marks nuclei. (F) Representative image of a murine Kras^{G12V}-driven lung tumor stained with phospho-p38 antibody. Scale bar, 200 μm. The histogram shows the percentage of phospho-p38^{+} cells in tumors and in healthy lung parenchymas (n=5 healthy tissues and 21 tumors from 6 different mice). Data represent average ± SEM.

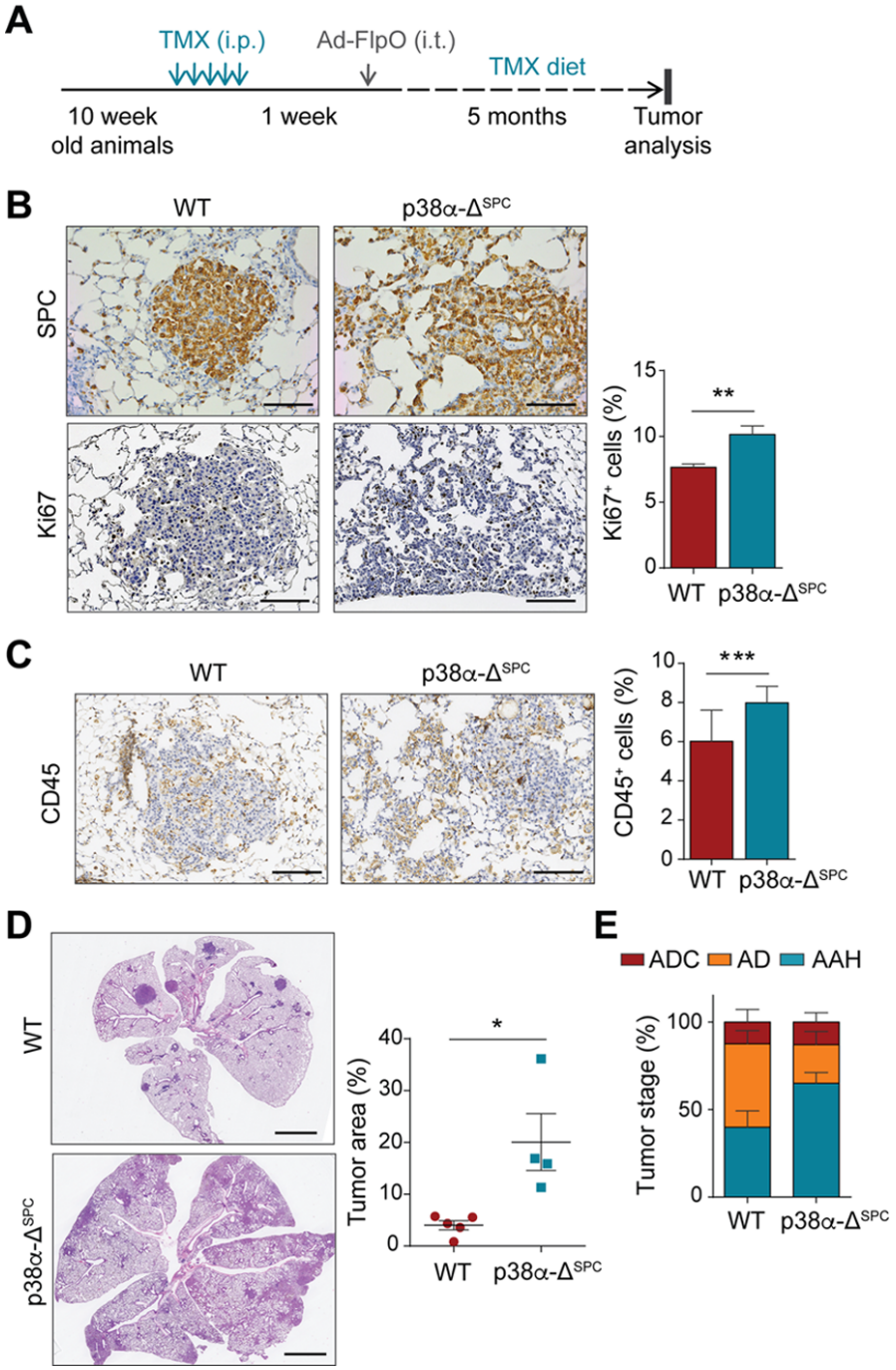

Fig. 2. p38α-Δ^{SPC} mice show increased tumor burden but delayed progression to advanced stages. (A) Schematic representation of the experimental treatment regime. Ad-FlpO, adenovirus expressing FlpO recombinase; TMX, tamoxifen; i.p., intraperitoneal injection; i.t. intratracheal administration. (B) Representative images of WT and p38α-Δ^{SPC} lungs stained for the AE2 marker SPC, or with Ki67 antibody to detect proliferative cells. Bar, 100 μm. The histogram

shows the quantification of the percentage of $Ki67^+$ cells per tumor (n=50 WT and 47 p38α-Δ^{SPC} tumors, from 5 different mice each). (C) Representative images of WT and p38α-Δ^{SPC} lungs stained with CD45 antibody to estimate the degree of immune cell infiltration. Bar, 100 μm. The histogram shows the quantification of the $CD45^+$ area as a percentage of the total area analyzed (n=30 WT and 56 p38α-Δ^{SPC} tumors, from 3 different mice each). (D) Representative images of WT and p38α-Δ^{SPC} lungs stained with H&E. Dot plots show the quantification of the tumor area (n≥4 mice). Bar, 2 mm. (E) Tumors were microscopically analyzed and classified according to their pathological stage as adenocarcinoma (ADC), adenoma (AD), and atypical adenomatous hyperplasia (AAH) (n≥4 mice). Data represent average ± SEM.

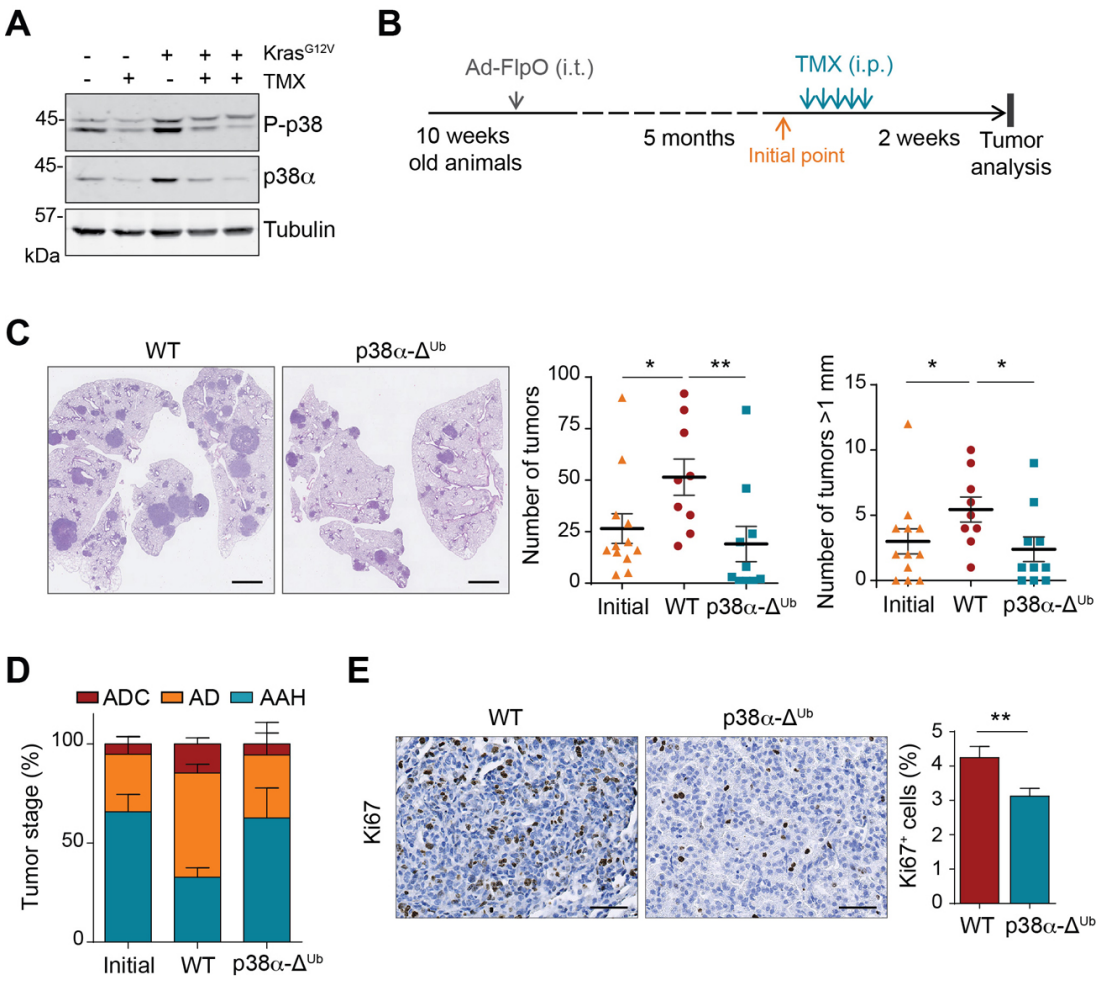

Fig. 3. p38α enables Kras^{G12V}-driven lung tumor progression. (A) Representative immunoblots with antibodies to p38α and phospho-p38 (P-p38) of whole lung lysates from WT and p38α-deficient mice, as indicated by - and + tamoxifen (TMX), respectively, either expressing or not Kras^{G12V}. Tubulin was used as loading control. Each line corresponds to one mouse. (B) Schematic representation of the experimental treatment regime. Ad-FlpO, adenovirus expressing FlpO recombinase; i.p., intraperitoneal injection; i.t. intratracheal administration. (C) Representative images of WT and p38α-Δ^{Ub} lungs stained with H&E. Bars, 2 mm. Dot plots show the quantification of both the tumor number and the number of tumors bigger than 1 mm in diameter per animal, before (Initial) and 2 weeks after the TMX treatment in WT and p38α-Δ^{Ub} mice (n≥9 mice per group). (D) Tumors as in (C) were microscopically analyzed and classified according to their pathological stage as adenocarcinoma (ADC), adenoma (AD), and atypical adenomatous hyperplasia (AAH). n≥6 mice per group. (E) Representative images of WT and

p38α-Δ^{Ub} lungs collected one week after TMX injections and stained with Ki67 antibody to detect proliferative cells. Bar, 100 μm. The histogram shows the quantification of $Ki67^{+}$ cells as a percentage of the total number of cells counted per tumor (n=37 WT and 27 p38α-Δ^{Ub} tumors, from 3 different mice each). Data represent average ± SEM.

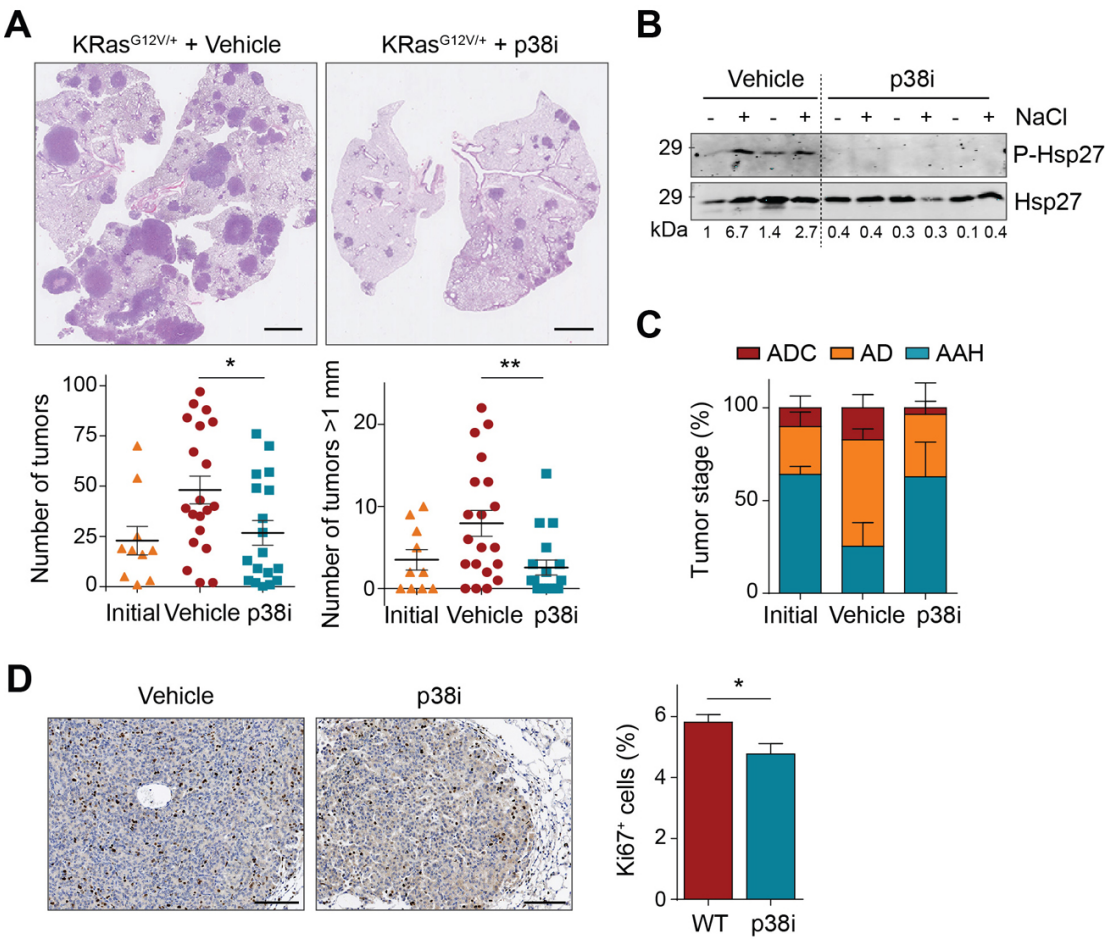

Fig. 4. Chemical inhibition of p38α impairs the growth of Kras^{G12V}-driven lung adenocarcinomas. (A) Representative images of H&E stained lungs from animals treated with vehicle or the p38α inhibitor PH797804 (p38i). Bar, 2 mm. Dot plots show the quantification of both the tumor number and the number of tumors bigger than 1 mm in diameter per animal, before (Initial) and after 2 weeks of treatment with vehicle or p38i. n≥10 mice per group. (B) Lungs with tumors from Kras^{G12V}-expressing animals that were administered vehicle or p38i for 15 days, were treated with NaCl ex vivo to hyperactivate the p38α pathway or left untreated, and then were immunoblotted with the indicated antibodies. Each pair of lines (- +) corresponds to one mouse. Representative examples are shown. (C) Tumors were microscopically analyzed and classified according to their pathological stage as adenocarcinoma (ADC), adenoma (AD), and atypical adenomatous hyperplasia (AAH). n=3 mice. (D) Representative images of lung tumors from animals treated with vehicle or p38i for 15 days that were stained with Ki67 antibody to detect proliferative cells. Bar, 100 μm. The histogram shows the quantification of Ki67^{+} cells per

tumor as a percentage of the total number of cells counted (n= 70 Vehicle- and 33 p38i-treated tumors, from 4 different mice each). Data represent average ± SEM.

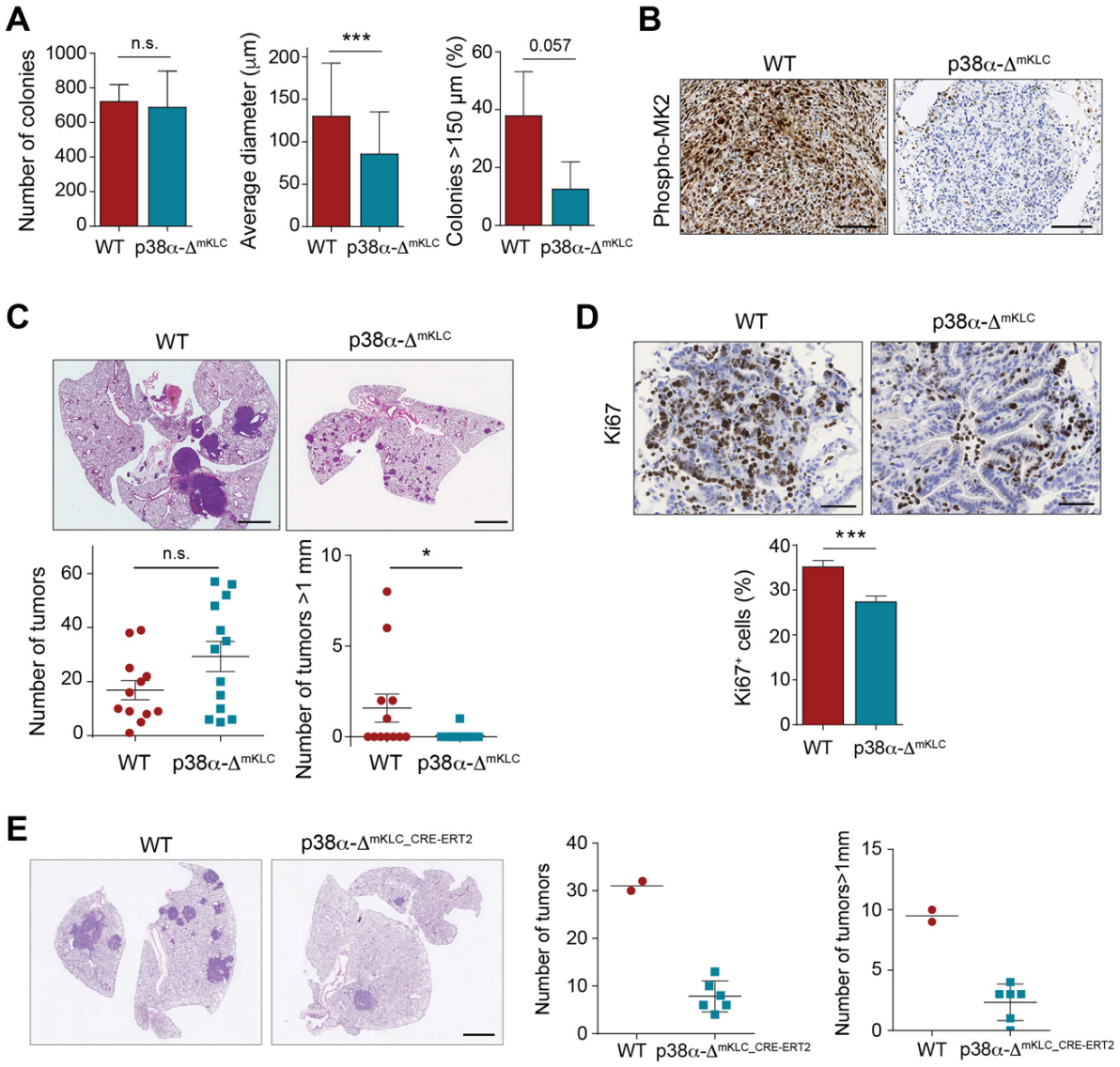

Fig. 5. Epithelial p38α is necessary for the proliferation of lung tumor cells. (A) WT and p38α-Δ^{mKLC} cells derived from mouse lung tumors were seeded in soft agar. Histograms show the number of colonies formed, their average diameter, and the percentage of colonies bigger than 150 μm per well (n≥42 colonies analyzed). Data represent mean ± SD. (B) Representative images of phospho-MK2 immunostainings of lung tumors formed by intratracheal inoculation of WT and p38α-Δ^{mKLC} cells. Bar, 100 μm. (C) Representative images of H&E stained lungs from WT animals that were intratracheally inoculated with either WT or p38α-Δ^{mKLC} cells. Bar, 2 mm. Dot plots show the average number of total tumors, and the number of tumors with a diameter bigger than 1 mm 22 days after the intratracheal inoculation (n≥12 mice per group). Data

represent average ± SEM. (D) Representative images of lung tumors from mice that were intratracheally inoculated with either WT or p38α-Δ^{mKLC} cells and were stained with Ki67 antibody. Bar, 100 μm. The histogram shows the quantification of $Ki67^{+}$ cells per tumor as a percentage of the total number of cells counted (n=55 WT and 70 p38α-Δ^{mKLC} tumors, each from ≥5 mice). Data represent average ± SEM. (E) Representative examples of lungs from mice that were intratracheally inoculated with either WT or p38α-$\Delta^{mKLC\_CRE\text{-}ERT2}$ cells, and 22 days later were treated with tamoxifen. Lungs were stained with H&E 15 days after p38α downregulation. Bar, 2 mm. Dot plots show the quantification of both the tumor number and the number of tumors bigger than 1 mm in diameter per animal (n=2-6 mice).

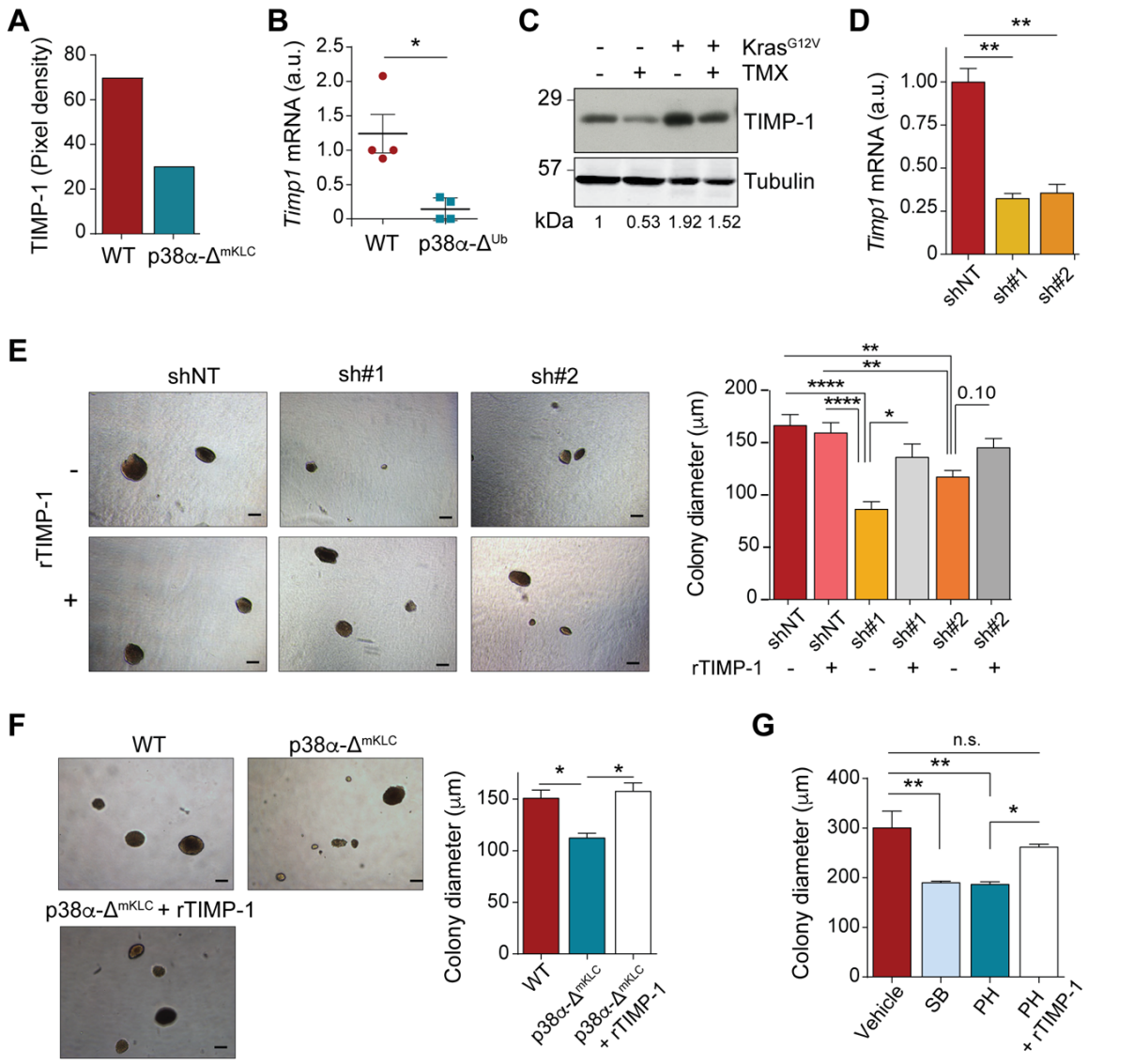

Fig. 6. p38α-regulated expression of TIMP-1 induces lung cancer cell proliferation. (A) Relative TIMP-1 protein levels in lung tumors from mice that were intratracheally inoculated with either WT or p38α-Δ^{mKLC} cells, as determined using a cytokine array (n=20 tumors from 4 mice per condition analyzed in a single array). (B) Relative *Timp1* mRNA expression in tumors from WT and p38α-Δ^{Ub} mice (n=4 tumors from ≥3 mice per group). (C) Representative immunoblots with antibodies to TIMP-1 and tubulin as a loading control of whole lung lysates from WT and p38α-Δ^{Ub} mice, as indicated by - and + tamoxifen (TMX), respectively, either expressing or not the *Kras*^{G12V} oncogene. Each line corresponds to one mouse. (D) Histogram showing *Timp1* downregulation in WT mKLC cells treated with shRNAs targeting *Timp1* (sh#1 and sh#2) or a

non-targeting control (shNT). (E) Representative images of the soft agar colonies formed by WT mKLC cells treated as in (D) in the presence or absence of recombinant TIMP-1 protein (rTIMP-1, 0.1 μg/ml) added twice a week. Bars, 150 μm. The histogram shows the average colony diameters (n≥52 colonies analyzed per group from 3 replicates). (F) Representative images of the soft agar colonies formed by WT cells, p38α-Δ^{mKLC} cells, and p38α-Δ^{mKLC} cells treated with rTIMP-1 protein (0.1 μg/ml) twice a week. Bars, 150 μm. The histogram shows the average colony diameters (n≥144 colonies analyzed per group from 6 replicates). (G) Average diameters of the colonies formed by the human NSCLC cell line H460 grown in soft agar for 20 days and treated with vehicle, the p38α inhibitors SB203580 (SB) and PH797804 (PH), or with PH plus 0.1 μg/ml rTIMP-1 protein (≥119 colonies analyzed per group from 3 replicates). Data represent mean ± SEM.

PNAS
www.pnas.org

Supplementary Information for

Requirement for epithelial p38α in KRAS-driven lung tumor progression

Jessica Vitos-Faleato, Sebastián M. Real, Nuria Gutierrez-Prat, Alberto Villanueva, Elisabet Llonch, Matthias Drosten, Mariano Barbacid, Angel R. Nebreda

Corresponding author: Angel R. Nebreda
Email: angel.nebreda@irbbarcelona.org

This PDF file includes:

Supplementary Methods

Biostatistical analysis of lung cancer patient cohorts. The gene expression omnibus (GEO) repository (1) was searched for microarray and survival data of NSCLC samples. The data set GSE10072 was processed in Bioconductor using RMA (2, 3) and the expression levels of the p38α encoding gene (*MAPK14*) in lung tumor samples and paired healthy parenchyma were analyzed. GSE31210 was used for determining *TIMP1* expression in relation to *MAPK14* levels. GSE8894 (series matrix data) and GSE30219 (RMA normalized adjusted data (4)) were used for assessing the prognostic value of *MAPK14*. The probe set used for *MAPK14* was 210449_x_at. Lung adenocarcinoma patient samples were split by median expression level and the two patient cohorts were compared by Kaplan–Meier survival plot, using Cox regression with 95% confidence intervals and log-rank P value with the R survival package 2.37.2.

Induction of Kras-driven tumors and p38α downregulation *in vivo*. Eight to twelve week old mice were intratracheally inoculated (5, 6) with a single dose (100 μl) of FLP recombinase-expressing adenovirus (10^9 pfu Ad-5CMV-FlpO/mouse, from Iowa University, Iowa, USA) under anesthesia (i.p. injection of 75 mg/kg ketamine, 1 mg/kg medetomidine, with a posterior recovery using 2 mg/kg atipamezol s.c.).

To activate the tamoxifen-inducible Cre recombinase, mice were intraperitoneally injected tamoxifen (12.5 mg/ml, Sigma #T5648), dissolved in a mix 1:9 of ethanol (Panreac): corn oil (Sigma). Doses of 0.125 mg/g body weight were injected for five consecutive days. p38α downregulation was confirmed one week after the last injection.

The inhibitor of p38α, PH797804 (Selleckchem #S2726) was dissolved at a concentration of 1.75 mg/ml in PBS containing 0.5% methylcellulose (Sigma) and 0.025% Tween20 (Sigma). Mice were weighed and a daily dose of 17.5 mg/kg body weight was administered by oral gavage for 15 consecutive days. Control mice were administered the vehicle solution. The inhibition of p38α was confirmed by immunoblotting 6 h after the last dose, using lysates of lungs incubated with or without NaCl (300 mM) for 15 min.

Cytokine array analysis of tumor lysates. Five dissected tumors from four different mice of each genotype were pooled together and lysed in 80 μl of buffer (PBS with 10 μg/ml aprotinin,

10 μg/ml leupeptin, and 10 μg/ml pepstatin) using the Precellys cell disruptor (Bertin Technologies). Triton X-100 was added to a final concentration of 1%, and lysates were frozen at -80°C overnight. Protein content was quantified for each pool with the DC Protein assay kit (BioRad) and 1.6 mg of protein were loaded onto the Cytokine profiler array membranes (R&D Systems #ARY006), following the manufacturer's instructions. Pixel densities on developed X-ray film were collected and analyzed using a transmission mode scanner and image analysis software (Image J).

Cell culture

Murine mKLC cells and LLC1 cells were maintained in DMEM (Sigma, #D5796). Human NSCLC cell lines H358 and H460 were grown in RPMI 1640 (Sigma, #8758). In all cases media was supplemented with 10% heat inactivated FBS (Thermo Fisher Scientific), 1% L-glutamine (Thermo Fisher Scientific) and 1% penicillin/streptomycin (Gibco), and cells were grown at 37°C and 5% CO2. All cell lines were tested for mycoplasma before performing the experiments by using the colorimetric kit from Lonza (#LT07-710).

For chemical inhibition of p38α, cells were treated every 24 h with PH797804 (1 μM; Selleckchem #S2726) or every 48 h with SB203580 (10 μM, Axon MedChem #1363). For IKK2 inhibition, cells were treated every 48 h with TPCA-1 (1 μM Sigma #T1452). Control cells were treated with DMSO vehicle.

Viral infections and shRNA-mediated knockdown

Cre-ERT2-expressing mKLC cells were generated by retroviral infection. Briefly, Cre-ERT2 was cloned into pWZL-blasticidin (Addgene #150477) and the resulting plasmid was co-transfected with pcL-Eco packaging vector (Addgene #12371) in HEK293T cells using $CaCl_2$ transfection. Culture supernatants were collected 48 h post-transfection, filtered (0.45 μm PVDF filter, Millipore), and centrifuged at 3000xg for 1 h at 4ºC (Amicon Ultra-15 #910024). Subconfluent mKLC cells were infected with one third of the recovered viral solution supplemented with 8 μg/ml polybrene (Sigma), and selected 48 h post-infection with 2 μg/ml blasticidin (Thermo Fischer Scientific #A1113903) added daily for 1 week.

The following shRNAs were obtained from Sigma: *Mapk14 #1* (TRCN0000023119), *Mapk14 #2* (TRCN0000310885), *Timp-1 #1* (TRCN0000080039), *Timp-1 #2,* (TRCN0000080042), Non-targeting control *(*SHC002). Lentivirus were produced in HEK293T cells co-transfected by $CaCl_2$ with third generation lentiviral plasmids from Addgene together with the shRNA-encoding plasmids. 48 h post-infection, cells were selected by daily addition of 1 μg/ml puromycin for 1 week.

Soft agar assays. Semisolid proliferation media contained either 0.35% or 0.5% agarose in DMEM or RPMI 1640 with 10% FBS. The bottom of 6-well plates was homogeneously covered with 0.5% agarose, and when solidified, 2000 lung cancer cells were mixed with an equal volume of 0.35% agarose in DMEM or RPMI 1640 and plated on top of the previous layer. After solidification of the second layer, 1 ml of DMEM or RPMI 1640 10% FBS was added, and renewed once a week. After 20-30 days, the number of colonies per well was manually counted under a microscope and photographed for size analysis with Image J software.

Adhesion, migration, anoikis and metastasis assays. Adhesion assays were performed in 24-well plates uncoated or coated with either 10 μg/ml fibronectin or 10 μg/ml collagen I. Cells were labeled with Cell Tracker Green (Invitrogen #C7025) for 30 min at 37°C, and then were incubated in DMEM 0.5% FBS overnight. $5x10^4$ cells in serum free media were added to each well of the 24-well plate, and after 2 h the wells were washed and adhered cells were fixed in formalin, photographed and counted.

To assay cell migration, $4x10^4$ cells, which had been grown overnight in DMEM 0.5% FBS, were seeded in DMEM 0.5% FBS on the upper part of Boyden chambers (Falcon #353097). The lower part of the chambers contained DMEM 10% FBS, or 0.5% FBS to be used as a control. After 20 h, the cells remaining on the upper part were removed, and the cells in the bottom part were fixed with 4% PFA, stained with crystal violet and counted.

To measure anoikis resistance, the bottom of a 24-well plate was coated with 120 μl of 0.03 g/ml poly-HEMA, and then $5x10^4$ cells were seeded per well. After 48 h, cells were stained with trypan blue and counted under the microscope.

For extravasation assays, HUVEC cells were grown for 4 days on the upper side of fibronectin pre-coated chambers (3 μm pore). LLC1 cells ($1x10^5$) were stained with Cell Tracker

Green (Invitrogen #C7025) and then were seeded on top of the HUVEC cells. After 12 h, the cells that were on the bottom part of the chamber were quantified.

To analyze metastatic dissemination, $4.5x10^5$ mKLC cells were subcutaneously injected into the rear flanks of 8-week old female athymic nude mice, and followed-up until they reached a maximum volume of 1 cm^3 using a caliper. Thereafter, tumors were removed, incisions were closed, and the mice were kept for 15 more days to monitor metastatic foci formation in distal organs.

In tail vein injection experiments, $9.5x10^5$ LLC1 cells were injected in six weeks-old nude mice and the tumor burden was determined by measuring the percentage of tumor area in H&E stained lung sections using computerized image software (Image J).

Flow cytometry assays. For the analysis of cell cycle profiles, trypsinized cells and their supernatant were centrifuged at 250xg for 5 min, washed with PBS and diluted to 10^6 cells/ml. 330 µl of the cell suspension were thoroughly mixed with 660 µl of ice-cold absolute ethanol added drop-wise. After overnight incubation at 4°C, pellet was resuspended in 500 µl of DNA staining solution containing 0.2 mg/ml RNase A (Roche #109-169) and 20 µg/ml propidium iodide (Sigma #P4864). Cells were incubated for 30 min at 30°C in a water bath in the dark, and then run in a Gallios flow cytometer (Beckman Coulter).

To measure BrdU incorporation, cells were pulsed for 90 min with 10 µM BrdU (Sigma #B9285), harvested, and resuspended in 500 µl PBS. 5 ml of cold 70% ethanol were added drop-wise while agitating the tube, and cells were stored overnight in the freezer. Cells were then pelleted, washed and their DNA was denatured with 0.5 ml of 0.1 M HCl, 0.5% Tween 20 for 10 min on ice and then washed and boiled. Cells were washed twice with 0.5% Tween, 1% BSA in PBS and then incubated with anti-BrdU-FITC antibody (BD Pharmingen #556028). After incubation for 30 min at RT in the dark, excess of antibody was washed out and cells were resuspended (10^6 cells in 400 µl) in PBS containing 2 mg/ml PI plus 5 mg/ml RNase A. Cell suspensions were run in a Gallios flow cytometer and analyzed using FlowJo software.

EpCAM expression was analyzed by incubating mKLC cells with EpCAM-FITC (Santa Cruz #53532, 1:50) for 30 min on ice in the dark. Samples were run in a Gallios flow cytometer (Beckman Coulter). DAPI (1:100) was used for exclusion of dead cells and debris and doublets

were excluded by plotting forward-scattered (FSC) versus side-scattered (SSC) channels. Data was analyzed using FlowJo software.

Immunoblotting. Lungs were harvested and immediately frozen in liquid nitrogen. A lobule was thawed on ice, mixed with lysis buffer (50 mM Tris–HCl pH 7.5, 150 mM NaCl, 1% NP-40, 5 mM EDTA, 5 mM EGTA, 20 mM NaF, 0.1 mM sodium orthovanadate, 1 mM DTT, 1 mM microcystin and the Protease Inhibitor Cocktail from Roche) and mechanically disrupted with a Precellys homogenizer (Bertin Technologies). The lysates were vortexed, incubated on ice for 10 min and centrifuged for 15 min at 16,000xg 4°C. Supernatants were quantified using the Protein Assay kit (Bio-Rad) and 40 μg of total protein were mixed with Laemmli buffer, separated by SDS-PAGE and transferred to nitrocellulose membrane (Whatman). The following antibodies were used: E-cadherin (BD Biosciences #610181; 1:1000), p38α (Cell Signaling #9218; 1:1000), phospho-Thr180/Tyr182 p38 (Cell Signaling #9211; 1:2000), Hsp27 (Santa Cruz #SC-1049; 1:1000), phospho-Ser82 Hsp27 (Cell Signaling #2401; 1:500), TIMP-1 (Cell Signaling #8946; 1:200) and tubulin (Sigma #T9026), which was used as loading control. Alexa Fluor 680 or 800-conjugated antibodies were used for detection (Invitrogen; 1:5000) and were visualized using Odyssey Infrared Imaging System (Li-Cor, Biosciences).

Analysis of *Mapk14* deletion. Genomic DNA was isolated from sorted cell populations or from lung tumors, and analyzed by qPCR with primers specific for exon 2 (floxed) and exon 12 (as a control) of the *Mapk14* gene encoding p38α. Relative amount of exon 2 versus exon 12 was determined. Primers are indicated in the two bottom rows of Table S1.

Quantitative RT-PCR. Total RNA was isolated from homogenized tumors, lung tissue, or isolated cells using the Purelink RNA minikit (Ambion #12183018A) following the manufacturer's instructions. The total RNA was then treated with DNase I and reverse transcribed using the Superscript IV system (Invitrogen) with random primers. qRT-PCR was carried out in triplicate using a BioRad CFX96™ thermal cycler machine with the SYBR Green method (Applied Biosystems). Relative levels of mRNAs were measured by the ΔΔC(t) method and normalized against the housekeeping genes encoding glyceraldehyde-3-phosphate

dehydrogenase (*Gapdh*) and hypoxanthine-guanine phosphoribosyltransferase (*Hprt1*). A complete list of the primers used is shown in Table S1.

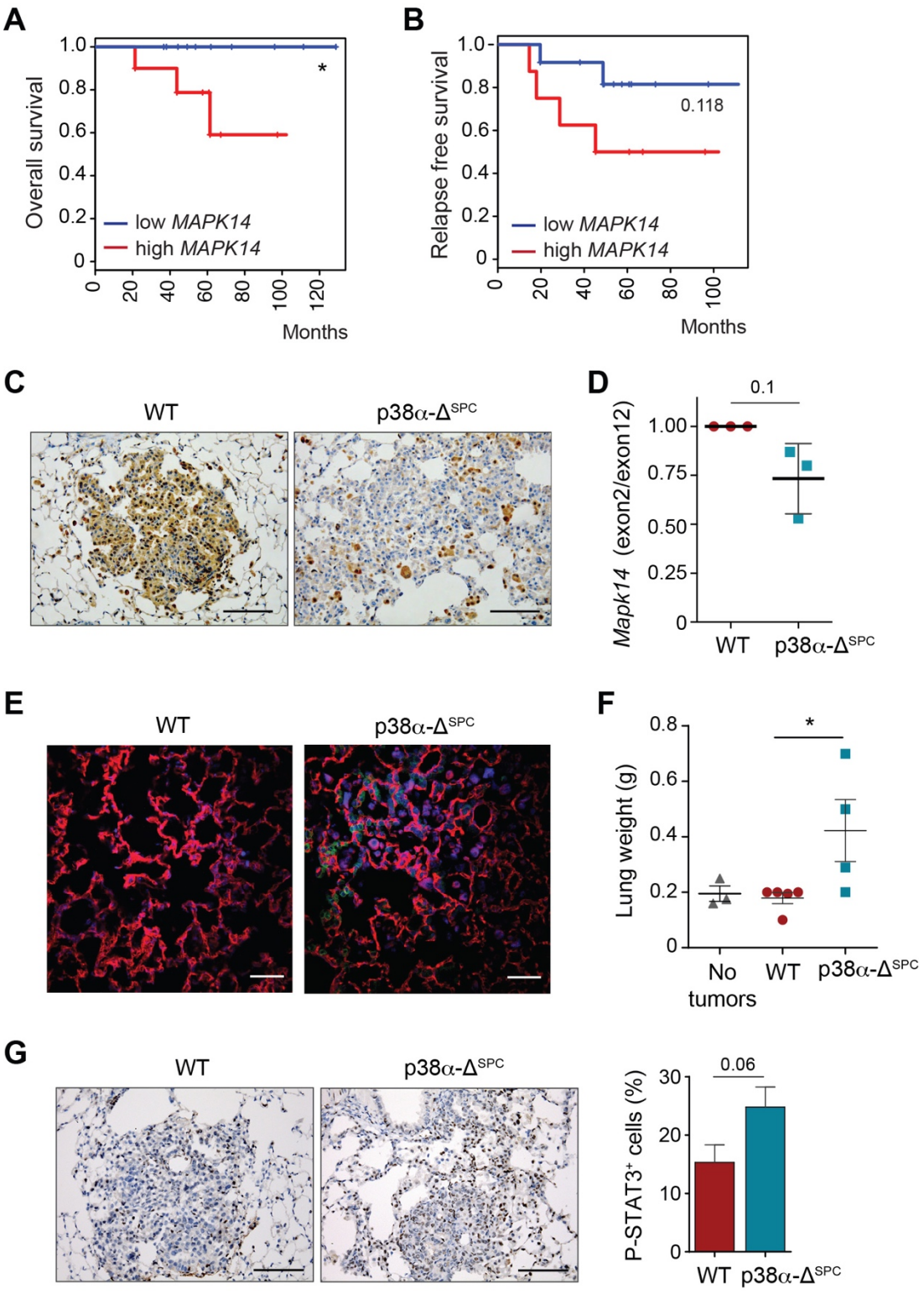

Fig. S1. KRAS-driven lung tumor prognosis correlates with *MAPK14* mRNA levels, but p38α-downregulation in lung progenitor cells enhances $Kras^{G12V}$-induced tumor size and inflammation. (A) Kaplan-Meier plots showing a univariate analysis of overall survival of KRAS-driven lung adenocarcinoma patients stratified by high or low *MAPK14* mRNA expression (n=10 per group).

(B) Kaplan–Meier plots displaying a recurrence-free survival over time of KRAS-driven lung adenocarcinoma patients stratified by high or low *MAPK14* mRNA expression (n≥8 per group). (C) Representative images of WT and p38α-Δ^{SPC} lungs stained with p38α antibodies. Bars, 100 μm. (D) WT and p38α-Δ^{SPC} mice were injected intraperitoneally with tamoxifen for 5 days and one week later AE2 cells were sorted as previously described ($CD31^-$ $CD45^-$ $ITGB2^+$ SPC^+ (7)). Genomic DNA was isolated and analyzed by qPCR for the relative copy number of exon 2 (floxed) versus exon 12 (control) of the p38α-encoding *Mapk14* gene (n=3 mice). (E) Representative images of lung sections from WT and p38α-Δ^{SPC} mice that constitutively express a fluorescent Tomato-eGFP reporter (8). Cells without and with Cre activity are red (Tomato) and green (eGFP), respectively. Nuclei were labeled with DAPI (blue). Scale bar, 50 μm. (F) Weights of the lungs from healthy mice (No tumors) and $Kras^{G12V}$-expressing WT and p38α-Δ^{SPC} mice (n≥3 mice). (G) Representative images of WT and p38α-Δ^{SPC} lungs stained with phospho-STAT3 antibodies. Bars, 100 μm. The histogram shows the quantification of phospho-$STAT3^+$ cells as a percentage of the total number of cells counted per tumor (n≥11 tumors from ≥3 mice per group). Data represent average ± SEM. $*P < 0.05$.

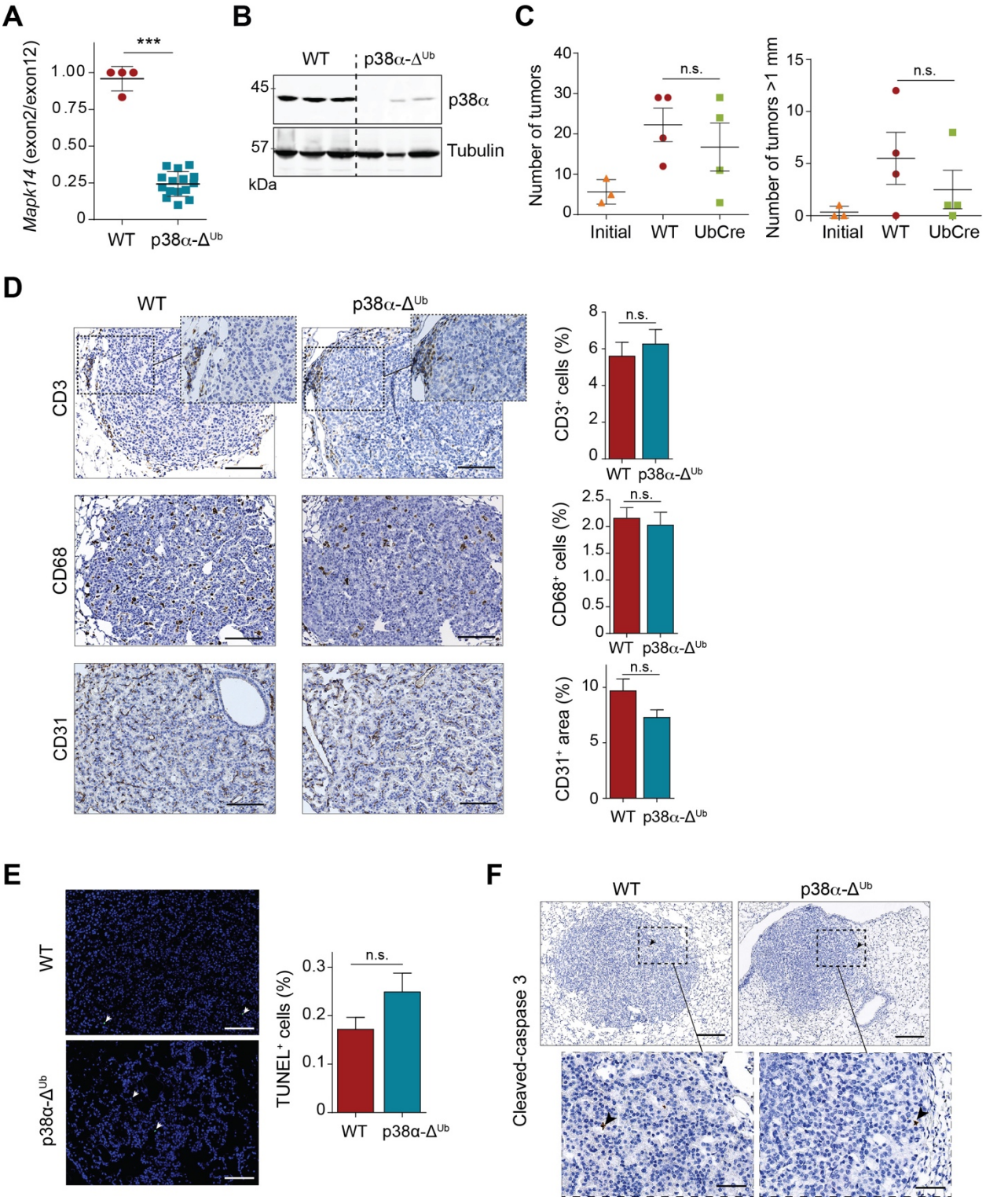

Fig. S2. p38α downregulation does not induce apoptosis, affect angiogenesis or impair immune infiltration in lung tumors. (A) Genomic DNA was isolated from individual tumors either from WT or p38α-Δ^{Ub} mice and the relative copy number of exon 2 (floxed) versus exon 12 (control) of the p38α-encoding *Mapk14* gene was analyzed by qPCR (n≥4 tumors). (B) Representative

immunoblots with antibodies to p38α and tubulin as a loading control from individual lung tumors that were collected one week after the tamoxifen treatment. Each line corresponds to one mouse. (C) Total number of tumors and number of tumors bigger than 1 mm in diameter before (Initial) and one week after tamoxifen treatment in *Mapk14*$^{+/+}$;Kras$^{+/FSFG12V}$ (WT) and *Mapk14*$^{+/+}$;UBC-Cre-ERT2;Kras$^{+/FSFG12V}$ (UbCre) mice (n≥3 mice). (D) Representative images of lung tumors from WT and p38α-Δ^{Ub} mice that were collected one week after the last tamoxifen injection and were analyzed for lymphocyte (CD3), alveolar macrophage (CD68) and endothelial cell (CD31) markers. Bars, 100 μm. The histograms show the quantifications as the percentages of stained surface per tumor (n≥19 tumors from ≥3 mice per group). (E) Representative images of lung tumors from WT and p38α-Δ^{Ub} mice stained for TUNEL. Stained cells are indicated with white arrowheads. Bars, 100 μm. The histogram shows the quantification of apoptotic cells as a percentage of the total number of cells counted per tumor (n≥24 tumors from ≥3 mice per group). (F) Representative images of lung tumors from WT and p38α-Δ^{Ub} mice stained for cleaved caspase 3. Stained cells are highlighted with black arrowheads. The indicated areas are magnified in the lower panels. Bars, 200 μm (upper) and 50 μm (lower). Data represent average ± SEM. ***$P < 0.001$, n.s. not significant.

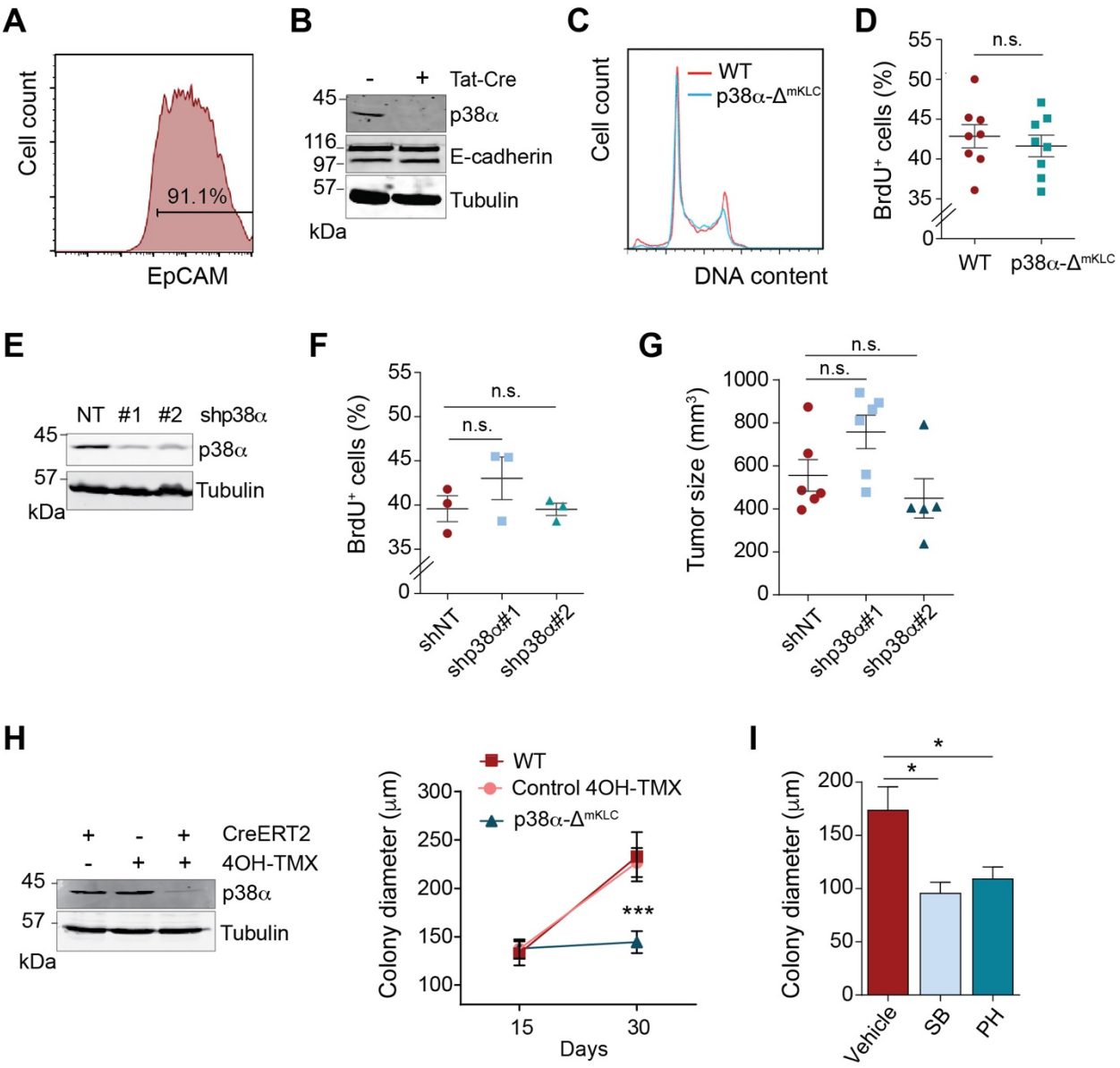

Fig. S3. p38α deficient lung cancer cells have impaired ability to grow in soft agar. (A) FACs analysis of mKLC cells for the EpCAM epithelial marker. (B) Representative immunoblots with antibodies to p38α, E-cadherin and tubulin as a loading control of WT and p38α-Δ^{mKLC} cells. (C) Representative cell cycle profiles of WT and p38α-Δ^{mKLC} cells. (D) WT and p38α-Δ^{mKLC} cells were labelled with BrdU and analyzed by flow cytometry (n=8). (E) Representative immunoblots of p38α expression in LLC1 cells expressing shRNAs targeting p38α (#1 and #2) or a non-targeting control (NT). Tubulin was used as loading control. (F) Cells in (E) were labelled with BrdU and analyzed by flow cytometry (n=3). (G) Six weeks-old female mice were injected subcutaneously into the rear flanks with $2x10^5$ LLC1 cells expressing shRNAs targeting p38α (#1 and #2) or a NT control, and tumor size was measured after 15 days (n≥5). (H) mKLC cells with *Mapk14* floxed alleles and either with or without Cre-ERT2, as indicated, were grown for 15 days in soft agar and colony diameters were measured. Then, 4-hydroxytamoxifen (4OH-TMX) was added or not to the culture media every 3 days and the colony diameters were

measured again two weeks later (n=3). Control 4OH-TMX indicates cells without Cre-ERT2 alleles that were treated with 4OH-TMX. Representative immunoblots of p38α expression in mKLC cells treated as indicated are shown in the left panel. Tubulin was used as loading control. (I) Diameter of the colonies formed by the human NSCLC cell line H358 grown in soft agar for 30 days in the presence of the p38α inhibitors SB203580 (SB) and PH797804 (PH) or vehicle (n≥104 colonies in each group from 3 replicates). Data represent average ± SEM. *$P < 0.05$, n.s. not significant.

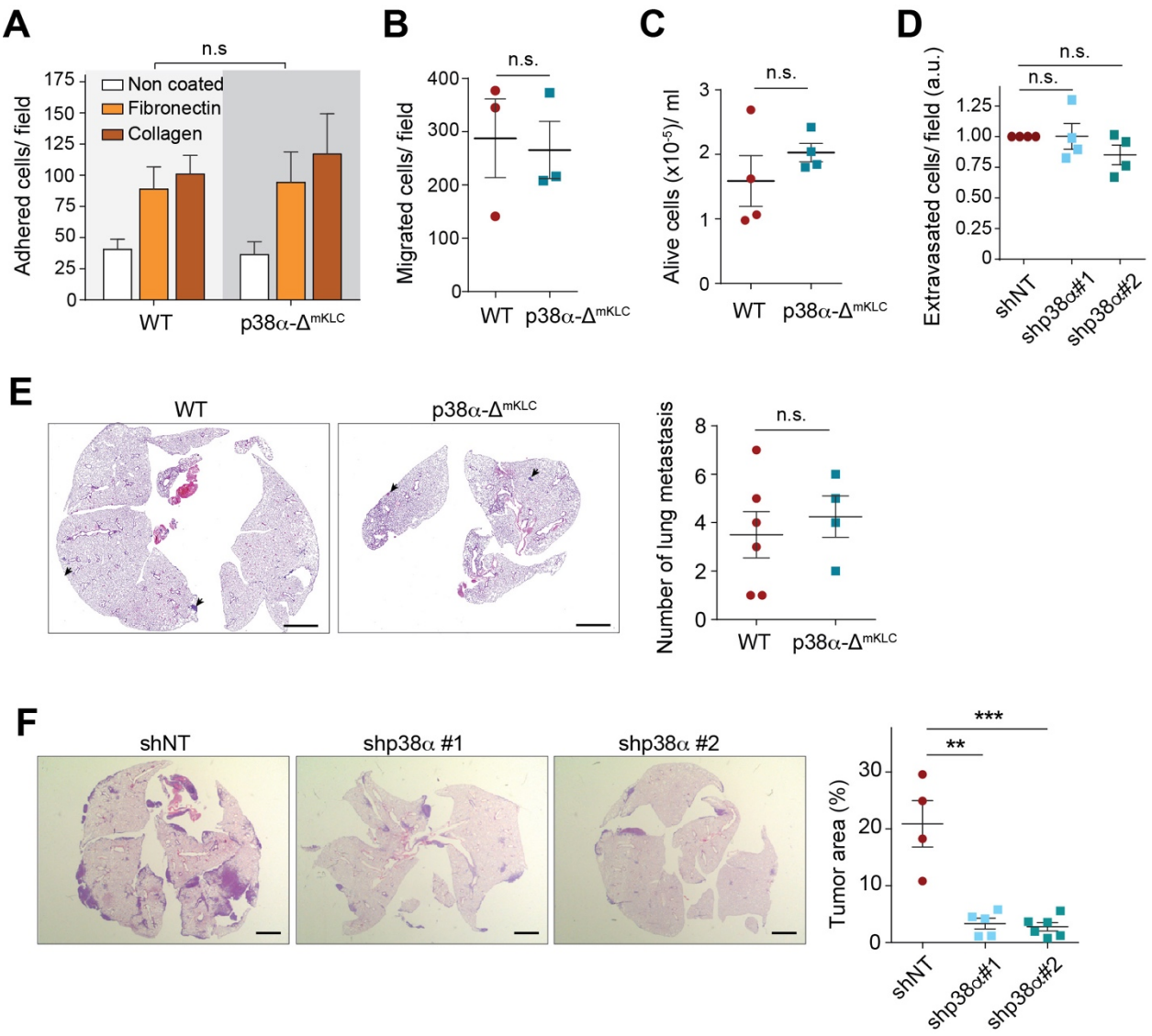

Fig. S4. p38α downregulation does not affect the metastatic properties of mKLC lung cancer cells but controls the growth of the tumor mass. (A) Number of WT and p38α-Δ^{mKLC} cells attached to uncoated, fibronectin-coated, and collagen-coated plates 90 min after seeding (n=8). (B) Number of WT and p38α-Δ^{mKLC} cells per field that migrated to the bottom of Boyden chambers after 20 h (n=3). (C) WT and p38α-Δ^{mKLC} cells were cultured for 48 h in non-adherent conditions to analyze anoikis resistance (n= 4). (D) LLC1 cells expressing shRNAs targeting p38α (#1 and #2) or a non-targeting control (NT) were seeded on Boyden chambers coated with fibronectin and HUVEC cells, and 12 h later the cells that extravasated to the lower part of the chamber were counted. Numbers are normalized to shNT cells (n=4). (E) Representative images of H&E stained lungs with metastatic foci formed in immunodeficient mice that were subcutaneously injected with WT or p38α-Δ^{mKLC} cells. Bar, 2 mm. Dot plots show the quantifications of the number of lung metastatic foci per mice counted 15 days after primary tumor resection (n≥4 mice). (F) Representative H&E staining of lungs 15 days after intravenous injection of LLC1 cells expressing shRNAs targeting p38α (#1 and #2) or a NT control. Bar, 2

mm. Percentage of tumor area relative to the total lung area in each mouse is indicated (n≥4 mice). Data represent average ± SEM. $^{**}P < 0.01$, $^{***}P < 0.001$, n.s. not significant.

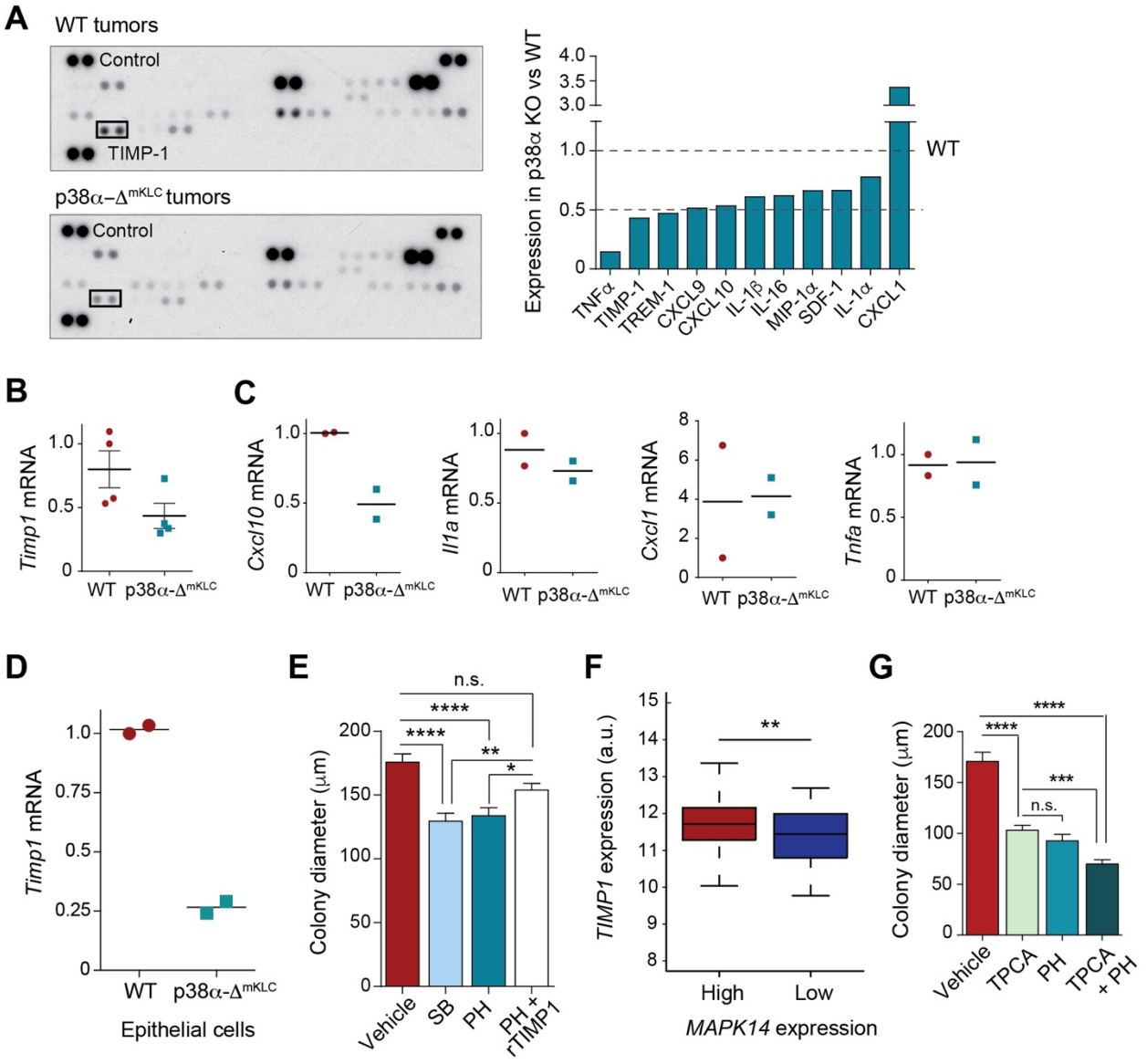

Fig. S5. TIMP-1 regulation by p38α controls lung cancer cell proliferation. (A) Twenty lung tumors from four different mice that were intratracheally inoculated with either WT or p38α-Δ^{mKLC} were lysed together and analyzed using a cytokine array. The histogram shows the fold change in pixel density of the ten most highly deregulated cytokines in p38α-Δ^{mKLC} tumors. Expression levels in WT tumors were given the value of 1. Internal array controls are indicated. (B) Analysis of *Timp1* mRNA expression by qRT-PCR in lung tumors from mice that were intratracheally inoculated with WT or p38α-Δ^{mKLC} cells (n=4). (C) Analysis of cytokines' mRNA expression by qRT-PCR in the lung tumors from WT or p38α-Δ^{mKLC} mice (n=2). (D) *Timp1* mRNA expression in lung epithelial cancer cells isolated from tumors of mice inoculated with WT or p38α-Δ^{mKLC} cells (n=2 mice). (E) Average colony diameters of mKLC cells grown in soft agar and treated with vehicle or the p38α inhibitors SB203580 (SB) and PH797804 (PH), either alone or together with 0.1 μg/ml of recombinant TIMP-1 protein (rTIMP1) added twice a week (n≥95 colonies analyzed per group from 3 replicates). (F) Boxplot for *TIMP1* mRNA levels

according to *MAPK14* mRNA levels in lung adenocarcinoma patient samples (n≥110 per group). (G) Average colony diameters of mKLC cells grown in soft agar and treated with either vehicle, the IKK2 inhibitor TPCA-1, the p38α inhibitor PH, or both together (n≥67 colonies analyzed per group from 3 replicates). Data represent average ± SEM. $*P < 0.05$, $**P < 0.01$, $***P < 0.001$, $****P < 0.0001$, n.s. not significant.

Table S1. Primers used for qPCR

Gene	Forward	Reverse
Cxcl1	CCTTGACCCTGAAGCTCCCT	CGGTGCCATCAGAGCAGTCT
Cxcl10	CCAAGTGCTGCCGTCATTTTC	GGCTCGCAGGGATGATTTCAA
Gapdh	CTTCACCACCATGGAGGAGGC	GGCATGGACTGTGGTCATGAG
Hprt	TCAGTCAACGGGGGACATAAA	GGGGCTGTACTGCTTAACCAG
Il1a	CGAAGACTACAGTTCTGCCATT	GACGTTTCAGAGGTTCTCAGAG
Timp1	GGTGTGCACAGTGTTTCCCTGTTT	TCCGTCCACAAACAGTGAGTGTCA
Tnfa	CGTCAGCCGATTTGCTATCT	CGGACTCCGCAAAGTCTAAG
Mapk14 exon 2	GCATCGTGTGGCAGTTAAGA	GTCCTTTTGGCGTGAATGAT
Mapk14 exon 12	GCCCTCCCTCACTTCAGGAG	TGTGCTCGGCACTGGAGACC

References

1. T. Barrett *et al*., NCBI GEO: archive for functional genomics data sets--update. *Nucleic Acids Res* **41**, D991-995 (2013).
2. R. C. Gentleman *et al*., Bioconductor: open software development for computational biology and bioinformatics. *Genome Biol* **5**, R80 (2004).
3. B. S. Carvalho, R. A. Irizarry, A framework for oligonucleotide microarray preprocessing. *Bioinformatics* **26**, 2363-2367 (2010).
4. A. C. Eklund, Z. Szallasi, Correction of technical bias in clinical microarray data improves concordance with known biological information. *Genome Biol* **9**, R26 (2008).
5. E. L. Jackson *et al*., Analysis of lung tumor initiation and progression using conditional expression of oncogenic K-ras. *Genes Dev* **15**, 3243–3248 (2001).
6. M. Puyol *et al*., A synthetic lethal interaction between K-Ras oncogenes and Cdk4 unveils a therapeutic strategy for non-small cell lung carcinoma. *Cancer Cell* **18**, 63-73 (2010).
7. R. T. Mukhametshina *et al*., Quantitative proteome analysis of alveolar type-II cells reveals a connection of integrin receptor subunits beta 2/6 and WNT signaling. *J Proteome Res* **12**, 5598-5608 (2013).
8. M. D. Muzumdar, B. Tasic, K. Miyamichi, L. Li, L. Luo, A global double-fluorescent Cre reporter mouse. *Genesis* **45**, 593-605 (2007).